Master's Thesis

Finite Temperature Renormalization in Luttinger Semimetals

Benedikt Poggel

Chair for Theoretical Solid State Physics
Faculty of Physics
Ludwig–Maximilians–Universität Munich

Supervised by Prof. Dr. Matthias Punk

February 3rd, 2021

Masterarbeit

Renormierung bei endlicher Temperatur in Luttinger-Halbmetallen

Benedikt Poggel

Lehrstuhl für theoretische Festkörperphysik
Fakultät für Physik
Ludwig–Maximilians–Universität München

Betreut von Prof. Dr. Matthias Punk

3. Februar 2021

Abstract

Systems with a quadratic band touching point (QBTP) as described by the Luttinger Hamiltonian [1] have been found to exhibit a zero-temperature non-Fermi liquid phase [2], commonly called the LAB (*Luttinger-Abrikosov-Beneslavsky*) fixed point. Its existence has been predicted using the dimensional regularization variant of the renormalization group. This thesis expands the calculations to finite temperatures: First, the LAB scaling is shown to be observable from the viewpoint of a random phase approximation. Second, dimensional regularization is applied to show that the flow equations don't acquire an explicit temperature dependence. Third, a momentum shell renormalization approach is pursued to derive full flow equations including temperature-dependent factors produced by the UV-finite terms neglected in dimensional regularization. The RPA exponent 1/2 of the bosonic mass turns out to be incorrect and evaluates numerically to about 1.1 in the momentum shell approach.

Contents

List of Figures

1. Introduction

In recent years, there has been substantial interest in the behavior of materials whose electronic dispersion exhibits a quadratic band touching point (QBTP) – that is to say, with $E \sim \pm k^2$ in the vicinity of the Γ point. This particular constellation is produced by a strong spin-orbit coupling leading to the inversion of an otherwise degenerate energy band. For crystals with cubic symmetry, the general Hamiltonian leading to a QBTP has first been derived by Joaquin Luttinger in 1956 [1] by the use of $k \cdot p$ theory. To ensure inversion symmetry is respected, it requires two pairs of doubly degenerate energy bands instead of just one non-degenerate upper and lower band. Materials with this feature are called *Luttinger semimetals*. They were later found to be of special interest because of their interesting phase diagram including topologically non-trivial as well as superconducting phases. An example for such a material – in fact the most promising one for the observation of the behavior described here – are pyrochlore iridates [2].

As early as in the 1970s, A. A. Abrikosov and S. D. Beneslavsky predicted a low-temperature phase with non-Fermi liquid behavior when combining the Luttinger Hamiltonian with a Coulomb interaction [3], later dubbed *Luttinger-Abrikosov-Beneslavsky* (LAB) phase, and calculated some of its critical indices [4]. Their work has been continued and expanded recently, induced by a modern formulation using renormalization group techniques by Eun-Gook Moon et al. [2]. Their paper provides the foundation for this thesis: it uses the dimensional regularization scheme [5][6][7] near the upper critical dimension $d = 4$ to find the renormalization group (RG) flow equations of the parameters defining the Hamiltonian which then lead to a stable non-Gaussian fixed point at a finite value of the interaction strength e. The work has been done perturbatively at one-loop level (order e^2) which is also the scope of this thesis – no calculations will be made beyond that order.

However, its emergence is a phenomenon found at zero temperature and it is not immediately clear how finite temperature will influence it. At the very least, it will appear as additional parameter in the renormalization procedure and result in a runaway flow in the parameter space. The goal of this project is to narrow down the concrete influence of finite temperature on the LAB phase addressing

the general question of whether and how the LAB phase survives and may be observable while also discussing possible temperature ranges for its existence. In particular, it tackles the open question how the thermal screening of the Coulomb interaction influences the LAB phase. We will pursue three approaches here: First, we encapsulate the finite temperature effects in a simple screened Coulomb potential and calculate its screening length in random phase approximation. Then, we estimate its impact by comparing it to the characteristic length scale of the LAB phase. Second, we will explore the original dimensional regularization approach at finite temperature and establish the flow equations. Finally, we will derive the RG flow again within a more intuitive momentum shell calculation encouraged by the fact that temperature doesn't change renormalization factors in dimensional regularization.

1.1. Remarks on Notation

All variable names used will be introduced and explained as needed. To ease the reading and achieve maximum notational transparency, it's useful to mention some of those used throughout the entire thesis here:

- ϵ designates the difference to the upper critical dimension 4, such that $\epsilon = 4 - d$ where d is the dimension of the system. Therefore, all equations containing d can be equivalently written in terms of ϵ and vice-versa.

- x and y will in general be used instead of multiple band masses for the Hamiltonian and the Green's functions. Their exact meaning is discussed in section 2.1. Both names won't be overloaded with different meanings – with the slight exception of subscripts for momentum components such as k_x which is never ambiguous.

- Outside of specific functions, $\vec{k}$ will be used to denote vector quantities and k for their absolute values. Deviations from this rule are made for clarity whenever context should make it clear what is meant. A common exception are the functions $d_a(k)$ and $p_c(k)$ introduced later which always depend on the vectorial quantity, not only its absolute value.

Furthermore, all calculations will be made in natural units $c = \hbar = k_B = 1$ unless explicitly stated otherwise. Thus, temperatures, masses etc. are to be thought as the corresponding energies. For the comparisons with the electrostatic energy, the charge e should always be measured in Gaussian units such that $\frac{e^2}{r}$ is the entire Coulomb energy. This implies that we need to scale the charge with the relative permittivity of the medium at hand or rather include sensible ranges for it when estimating energies.

2. The Zero-Temperature LAB Phase

In this chapter, the system will be presented in its path integral formulation starting with the Hamiltonian. Then, the calculations made by Moon et al. in [2] and its supplementary material will be retraced and the gaps closed – they omit most steps and give only results along with their general approach. This chapter lies the groundwork for the analogous calculations at finite temperature in chapter 4.

2.1. The System

The Luttinger Hamiltonian can be derived using $k \cdot p$-theory up to the second order when imposing cubic and inversion symmetry [1]. A four-dimensional representation is needed to obtain a QBTP since in any two-dimensional one, the degeneracy of the two branches of the dispersion can't be broken. This is because the energy must be independent of the spin direction of electron which requires a two-fold degeneracy of each band. The natural form explicitly showing the symmetries of the Hamiltonian uses the four-dimensional $J = 3/2$ spin matrices, J_x, J_y and J_z [2, supplemental material]:

$$H(\vec{k}) = \alpha_1 k^2 + \alpha_2(\vec{k} \cdot \vec{J})^2 + \alpha_3(k_x^2 J_x^2 + k_y^2 J_y^2 + k_z^2 J_z^2) \tag{1}$$

The three addends are the second-order invariants under cubic symmetry (with only the third breaking the invariance under arbitrary rotations), the α_i are commonly called *Luttinger parameters*. For actual calculations, it is more convenient to switch to a set of band masses directly involved in the dispersion by introducing a set of five 4×4 gamma matrices Γ_a generating a Clifford algebra. They obey the anticommutation relations

$$\{\Gamma_a, \Gamma_b\} = 2\delta_{ab} \tag{2}$$

and can be computed explicitly as products of the spin matrices [8].

$$
\begin{aligned}
\Gamma_1 &= \frac{1}{\sqrt{3}}(J_y J_z + J_z J_y) \\
\Gamma_2 &= \frac{1}{\sqrt{3}}(J_x J_z + J_z J_x) \\
\Gamma_3 &= \frac{1}{\sqrt{3}}(J_x J_y + J_y J_x) \\
\Gamma_4 &= \frac{1}{\sqrt{3}}(J_x^2 - J_y^2) \\
\Gamma_5 &= J_z^2 - \frac{5}{4}
\end{aligned}
\tag{3}
$$

While the first three of these matrices appear directly in the second term of equation 1, the fourth and fifth will combine for the non-mixed terms by the use of $J_x^2 + J_y^2 + J_z^2 = 15/4 \cdot \mathbb{1}$. The Hamiltonian then takes the following form with three "band masses" m, M_0 and M_c whose meaning will be discussed shortly after obtaining the eigenenergies [2].

$$
H = \frac{d^a(k)\Gamma_a}{2m} + \frac{k^2}{2M_0} + \frac{d^4(k)\Gamma_4 + d^5(k)\Gamma_5}{2M_c} \tag{4}
$$

Here, five momentum functions $d_a(k)$ have been introduced in analogy to (3):

$$
\begin{aligned}
d_1(k) &= -\sqrt{3}k_y k_z \\
d_2(k) &= -\sqrt{3}k_x k_z \\
d_3(k) &= -\sqrt{3}k_x k_y \\
d_4(k) &= -\frac{\sqrt{3}}{2}(k_x^2 - k_y^2) \\
d_5(k) &= -\frac{1}{2}(2k_z^2 - k_x^2 - k_y^2)
\end{aligned}
\tag{5}
$$

To improve readability, $d_a(k)$ instead of $d_a(\vec{k})$ is understood throughout the thesis. Similarly, $d_a(k+q)$ as it appears later should be read as $d_a(\vec{k}+\vec{q})$. Returning to the Hamiltonian, diagonalization is achieved easily by separating the part proportional to the unit matrix (second addend) and squaring the rest which yields a diagonal matrix due to the anticommutation relation (2). The resulting dispersion

features two branches, each with a two-fold degeneracy.

$$\begin{aligned} E_{\pm}(k) &= \frac{k^2}{2M_0} \pm \sqrt{\left(\frac{k^2}{2m}\right)^2 + \frac{m+2M_c}{4mM_c^2} p_c(k)} \\ &=: E_0(k) \pm \Delta_E(k) \end{aligned} \tag{6}$$

Here, $p_c(k) = \sum_i k_i^4 - \sum_{i<j} k_i^2 k_j^2$ encodes the cubic anisotropy – it takes the largest values along the coordinate axes. The anisotropic band mass M_c controls its strength (with larger M_c corresponding to less anisotropy). For the system to exhibit a QBTP, $M_0 > m$ is required such that the branches have different signs – M_0 breaks the symmetry between the lower and upper branch and is therefore associated with particle-hole asymmetry. For all future calculations, it is useful to pass to another set of parameters, namely the mass ratios $x = m/M_c$ and $y = m/M_0$, and separate the dependences on the absolute value of the momentum $\vec{k}$ and its direction.

$$E_{\pm} = \frac{k^2}{2m}\left(y \pm \sqrt{1 + x(2+x)p_c(\hat{k})}\right) \tag{7}$$

Here, $\hat{k}$ denotes the unit vector in $\vec{k}$ direction. The band mass m controls the general scale of the dispersion – it is the only one that needs to be finite in order for a QBTP to exist. y will be called *particle-hole asymmetry*: at $y = 0$, the upper and lower branches of the dispersion only differ in sign and are otherwise symmetric upon reflection on the k axis. The previously mentioned condition on the mass M_0 translates into $y < 1$. Otherwise, the lower branch of the dispersion will no longer be negative and "flip", effectively destroying the QBTP. x controls the degree of cubic anisotropy in the system. While the $x = 0$ model is completely isotropic (invariant under arbitrary rotations of the 3-dimensional space), $x \neq 0$ breaks this symmetry to a cubic one by turning on $p_c(k)$ – the system then will be invariant only under the associated discrete set of rotations and inversions. The mass ratio x must be positive, but otherwise has no upper bound. It will turn out that the LAB fixed point has both x and y at zero. The dependence of the dispersion on x and y is qualitatively displayed in figure 1.

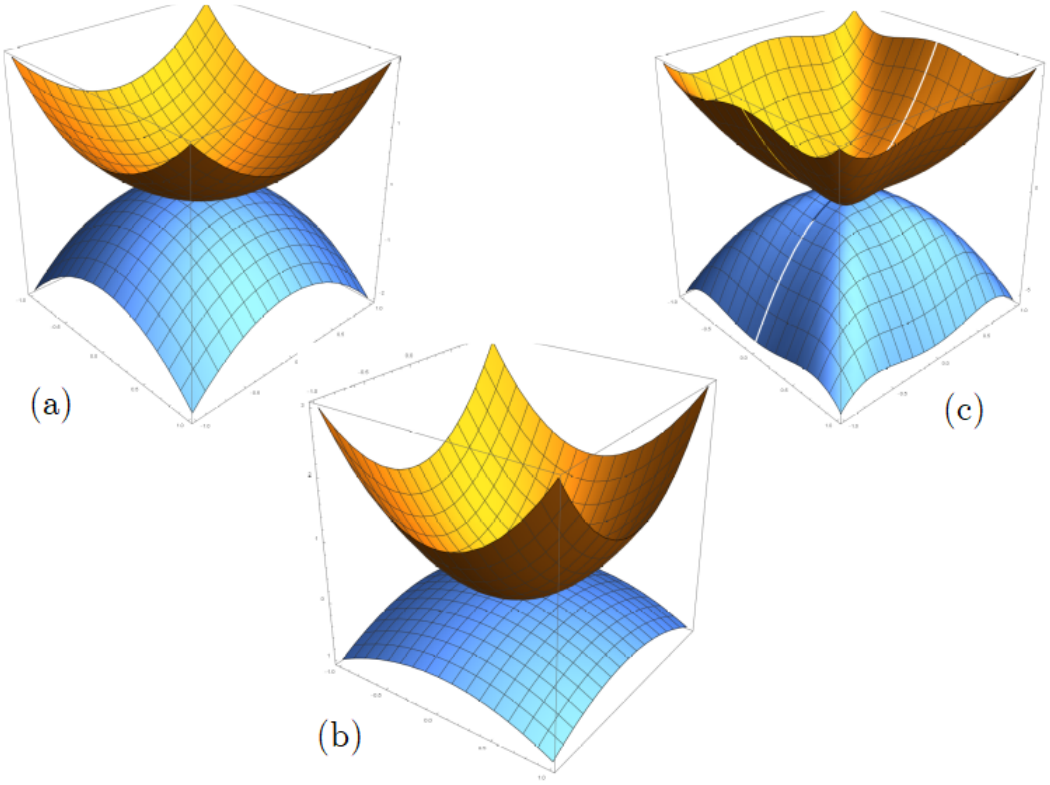

Figure 1: Qualitative plots of the dispersion in the k_x-k_y plane. The orange surface represents the upper branch, blue the lower one. (a) has $x = y = 0$, (b) $y \neq 0$ and (c) $x \neq 0$.

2.2. Action and Green's Functions

Together with the Coulomb interaction, the action functional for the Luttinger semimetal reads as follows in the euclidean path integral formulation. The interaction is mediated by a bosonic field φ.

$$S = \int d\tau d^d x \left\{ \Psi^\dagger(x,\tau) \left(\partial_t - i\tilde{e}\varphi + H(-i\vec{\nabla}) \right) \Psi(x,\tau) + \frac{1}{8\pi} \partial_i \varphi(x,\tau) \partial^i \varphi(x,\tau) \right\} \tag{8}$$

Here, $\tilde{e}$ designates the interaction strength, Ψ the fermionic and φ the bosonic field. $H(-i\vec{\nabla})$ denotes the Hamiltonian with $\vec{k}$ replaced by $-i\vec{\nabla}$. All calculations will be performed in a frequency-momentum representation obtained with a Fourier transformation. After inserting the Hamiltonian (4), it takes the form

$$S = \int_q \sum_\omega \Psi^\dagger(q,i\omega)\left(-i\omega + \frac{q^2}{2M_0} + \sum_{a=1}^{3}\frac{d_a(q)\Gamma^a}{2m} + \sum_{a=4}^{5} d_a(q)\Gamma^a\left(\frac{1}{2m}+\frac{1}{2M_c}\right)\right)\Psi(q,i\omega)$$
$$- ie\mu^{\frac{\epsilon}{2}}\int_{q,k}\sum_{\omega,\Omega}\Psi^\dagger(q+k,i\omega+i\Omega)\varphi(k,i\Omega)\Psi(q,i\omega)$$
$$+\frac{1}{8\pi}\int_k\sum_\Omega \varphi(-k,-i\Omega)k^2\varphi(k,i\Omega). \quad (9)$$

In this equation, the integrals over momenta have been abbreviated as $\int_k \equiv \int \frac{d^dk}{(2\pi)^d}$. The sums over frequencies are to be replaced either by integrals in the zero temperature case ($\sum_\omega \equiv \int \frac{d\omega}{2\pi}$) or by sums over fermionic (ω) or bosonic (Ω) Matsubara frequencies at finite temperature ($\sum_\omega f(\omega) \equiv 1/\beta \sum_i f(\omega_i)$). In preparation for the RG calculations within the dimensional regularization scheme, a momentum scale μ has been introduced to keep the canonical dimension of the new interaction parameter $e = \tilde{e}\mu^{-\epsilon/2}$ fixed when the dimensionality of the system varies. The correct power of μ is determined by the canonical dimensions given in (12). As mentioned in the introduction, $\epsilon = 4 - d$ denotes the deviation from the upper critical dimension 4 where the interaction becomes irrelevant in the RG sense. The first line represents the noninteracting electrons with the QBTP dispersion, the second line incorporates the Coulomb interaction via a bosonic field and the third one the free ("kinetic") energy of that field.

For the calculation of the self energies, we need the fermionic and bosonic Green's functions, G_f and G_φ respectively. The explicit form of G_f can be obtained with a multiplication similar to the diagonalization of the Hamiltonian.

$$G_\varphi(\vec{k},\Omega) = \frac{4\pi}{k^2} \quad (10)$$

$$\begin{aligned} G_f(\vec{k},\omega) &= (-i\omega + H)^{-1} \\ &= \frac{\left(-i\omega + \frac{k^2}{2M_0}\right) - \frac{d_a(k)}{2m}\Gamma^a - \frac{d_4(k)\Gamma^4 + d_5(k)\Gamma^5}{2M_c}}{\left(-i\omega + \frac{k^2}{2M_0}\right)^2 - \frac{k^4}{(2m)^2} - \frac{m+2M_c}{4mM_c^2}p_c(\vec{k})} \\ &= \frac{(-i\omega + E_0) - \frac{d_a(k)}{2m}\Gamma^a - \frac{d_4(k)\Gamma^4 + d_5(k)\Gamma^5}{2M_c}}{(-i\omega + E_0^2)^2 - \Delta_E^2} \end{aligned} \quad (11)$$

It is to note that the bosonic Green's function carries no frequency dependence. Computations involving the general fermionic propagator tend to become quite cumbersome, therefore it will often be necessary to consider the case $M_0, M_c \to \infty$ (equivalently $x = y = 0$) to simplify the Green's function.

2.3. T=0 Renormalization Group

To find the LAB phase at zero temperature, we employ the method of dimensional regularization to derive the RG flow: We compute the one-loop diagrams at arbitrary dimension d and continue the expression to non-integer dimensions. Working close to the upper critical dimension 4 yields a small expansion parameter $\epsilon = 4-d$, to be taken into account up to first order. The one-loop diagrams will then show a UV divergence of order $1/\epsilon$. Following a minimal subtraction scheme [6][7], these infinities will be subtracted from the action, resulting in so-called Z-factors of the form $1 + C/\epsilon$. The original form of the action needs to be restored thereafter by rescaling the appearing quantities (fields and couplings) with appropriate powers of the Z-factors. The couplings then flow with the arbitrary momentum scale μ introduced earlier. Finally, one obtains their flow equations and can solve them for fixed points which may depend on ϵ. Eventually a non-Gaussian fixed point will emerge at finite values of ϵ.

As a first step, the canonical dimensions of all fields and parameters in the action need to be determined. Under the condition that the action needs to be dimensionless (working in natural units), they evaluate as given in (12). One dimension can be taken as reference, it is convenient to choose $[k] = 1$.

$$
\begin{aligned}
[k] &= 1 \\
[\omega] &= z \\
[\Psi] &= -\frac{d}{2} - z \\
[\varphi] &= -\frac{2+z+d}{2} \\
[e] &= \frac{z-2}{2} \\
[m] &= [M_c] = [M_0] = 2 - z
\end{aligned}
\tag{12}
$$

Here, z is the dynamical exponent to be determined during the renormalization procedure. In the noninteracting case, ω scales with k^2 such that $z = 2$.

To proceed, we will calculate all three one-loop diagrams displayed in figure 2. These comprise the bosonic and fermionic self energies as well as the vertex correction, each corresponding to one of the three integrals in the action (9) and determining their associated Z-factors. To simplify, all finite contributions can be dropped since only the parts that diverge for $\epsilon \to 0$ are needed for the counterterms in the minimal subtraction scheme. The fermionic Green's functions will be parametrized from the start using the parameters $x = m/M_c$ and $y = m/M_0$ instead of the band masses M_c and M_0.

$$
\begin{aligned}
G_f(\vec{k},\omega) &= 2m\frac{(-2mi\omega + yk^2) - d_a(k)\Gamma^a - x(d_4(k)\Gamma^4 + d_5(k)\Gamma^5)}{(-2mi\omega + yk^2)^2 - k^4 - x(2+x)p_c(\vec{k})} \\
&=: 2m\frac{(-2mi\omega + e_0(k)) - d_a(k)\Gamma^a - x(d_4(k)\Gamma^4 + d_5(k)\Gamma^5)}{(-2mi\omega + e_0(k))^2 - \delta_E(\vec{k})^2}
\end{aligned}
\tag{13}
$$

To shorten future equations, the abbreviations $e_0 = 2mE_0 = yk^2$ and $\delta_E = 2m\Delta_E = k^2\sqrt{1 + x(2+x)p_c(\hat{k})}$ have been introduced.

2.3.1. Bosonic Self Energy

We start with the bosonic self energy. Its diagram is given by

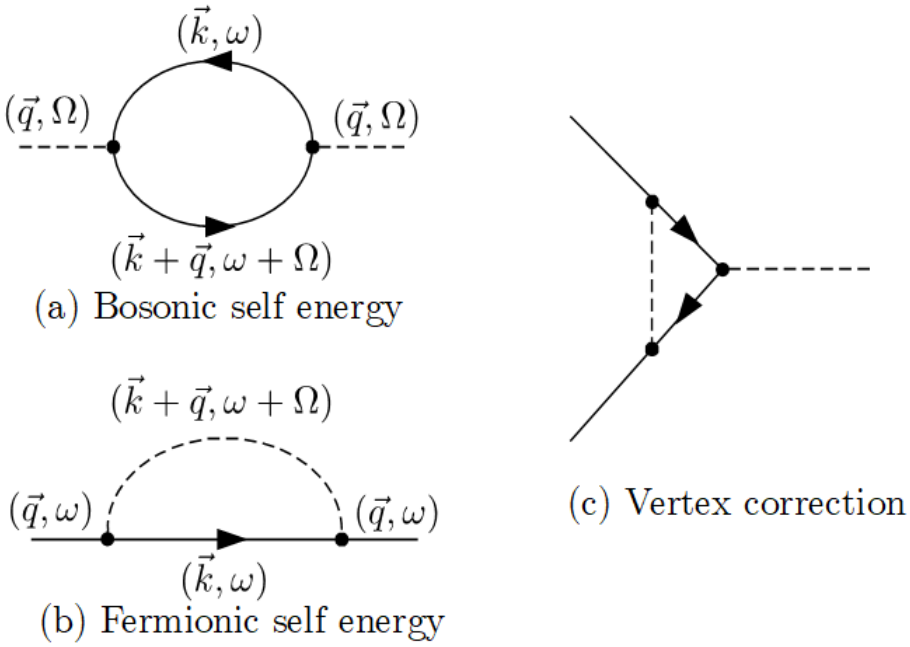

Figure 2: The one-loop diagrams necessary to be calculated. Dashed lines represent bosonic Green's functions, unbroken lines fermionic ones. All diagrams are to be calculated in amputated version, that is, without Green's functions for the external legs. Momentum designations have been omitted for the vertex correction for space reasons and because it won't be calculated explicitly in the main text. A fully annotated diagram can be found in figure 16 in the appendix.

$$\Sigma_\varphi(\vec{q},\Omega) = -e^2\mu^\epsilon \int \frac{d^dk}{(2\pi)^d} \int \frac{d\omega}{2\pi} \operatorname{Tr}\left\{G_f(\vec{k},i\omega)G_f(\vec{k}+\vec{q},i\omega+i\Omega)\right\}. \tag{14}$$

Because the gamma matrices and combinations of the form $\Gamma_a\Gamma_b$ with $a \neq b$ are traceless, only terms proportional to the identity matrix survive the trace. The Ω dependence is subdominant [2] and irrelevant to the Z-factor, hence we will set $\Omega = 0$. After resolving the trace and plugging in the Green's functions, we obtain

$$\Sigma_\varphi(\vec{q},0) = -16(me)^2\mu^\epsilon \int \frac{d^dk}{(2\pi)^d}\int\frac{d\omega}{2\pi}$$
$$\frac{[-2mi\omega + e_0(k)][-i2m\omega + e_0(k+q)] + d_a(k)d^a(k+q) + x(2+x)[d_4(k)d_4(k+q) + d_5(k)d_5(k+q)]}{[(-2mi\omega + e_0(k)^2)^2 - \delta_E(k)^2][(-2mi\omega + e_0(k+q)^2)^2 - \delta_E(k+q)^2]}. \tag{15}$$

The product of d_a-functions in the numerator can now be resolved by using

$$\begin{aligned} d_a(k)d^a(p) &= \frac{3(\vec{k}\cdot\vec{p})^2 - k^2p^2}{2} \\ d_4(k)d_4(p) + d_5(k)d_5(p) &= \sum_i k_i^2p_i^2 - \frac{1}{2}\sum_{i\neq j} k_i^2p_j^2 =: \widetilde{p_c}(k,p). \end{aligned} \tag{16}$$

The abbreviation in the last line has been chosen to emphasize the close relation to the cubic anisotropy function $p_c(k) = \widetilde{p_c}(k,k)$ appearing in the dispersion.

To proceed, we will perform a Taylor expansion in small q under the integral. The constant term vanishes upon frequency integration because of the second-order pole in $z = 2mi\omega$. Turning to the derivatives of the integrand, it is important to note that it only depends on the momenta through k^2, $p_c(k)$ and the two combinations in (16) with $p = k + q$. It is

$$\begin{aligned} \frac{d}{dq_i} d_a(k)d^a(k+q)|_{q=0} &= 2k^2k_i \\ \frac{d}{dq_i}[d_4(k)d_4(k+q) + d_5(k)d_5(k+q)]|_{q=0} &= 2k_i^3 - k_ik_\perp^2 \\ \frac{d}{dq_i}(\vec{k}+\vec{q})^2|_{q=0} &= 2k_i \\ \frac{d}{dq_i}p_c(k+q)|_{q=0} &= 4k_i^3 - 2k_ik_\perp^2. \end{aligned} \tag{17}$$

where $k_\perp^2$ is the squared absolute value of the components perpendicular to k_i. These inner derivatives cause each linear term in the Taylor expansion being antisymmetric in one component of the integration variable k. The first order

therefore vanishes after the momentum integration. The same is true for the mixed terms of the second order since they remain antisymmetric in at least one momentum component. Hence, only the isotropic contribution $\sim q^2$ doesn't vanish at this order. This is an implication of cubic symmetry which doesn't allow other (scalar) contributions.

Calculating the second-order term is straightforward, but cumbersome in the general case of $x \neq 0, y \neq 0$. Therefore, we first turn to the case $x = y = 0$. The self energy reads

$$\Sigma_\varphi(\vec{q}, 0) = -16(me)^2\mu^\epsilon \int \frac{d^dk}{(2\pi)^d} \int \frac{d\omega}{2\pi} \frac{(2mi\omega)^2 + k^4 + \frac{3\cos^2\theta - 1}{2} k^2q^2}{((2mi\omega)^2 - k^4)((2mi\omega)^2 - (\vec{k} + \vec{q})^4)}. \quad (18)$$

θ denotes the angle between the $\vec{k}$ and $\vec{q}$ vectors: $kq\cos\theta = \vec{k} \cdot \vec{q}$. Expanding to second order and dropping the constant and first order terms for the reasons explained above yields

$$\Sigma_\varphi(\vec{q}, 0) = -4me^2\mu^\epsilon \int \frac{d^dk}{(2\pi)^d} \int \frac{dz}{2\pi i} \frac{k^2((-5 + 27\cos^2\theta)k^8 + 2k^4z^2(1 + 13\cos^2\theta) + z^4(3 + 11\cos^2\theta))}{(z^2 - k^4)^4} \times q^2. \quad (19)$$

In preparation for the frequency integration, ω has been substituted by $z = 2mi\omega$. It can then be resolved via the residue theorem. This is straightforward in principle despite the complex form of the numerator and the high order of z in the denominator. The poles are located at the eigenenergies of the Hamiltonian, $z = \pm k^2$. The integrand falls off $\sim z^{-4}$ at infinity such that the contour can be closed in either half plane – one pole will then fall within the enclosed region.

$$\Sigma_\varphi(\vec{q}, 0) = -3me^2\mu^\epsilon \int \frac{d^dk}{(2\pi)^d} \frac{5\cos^2\theta - 1}{k^4} \times q^2 \quad (20)$$

In analogy to Moon et al. [2], the general d-dimensional integral will be resolved in a manner that respects the cubic symmetry only defined in $d = 3$. The angular part of the integral will first be resolved in three dimensions. Then, general di-

mensionality d will be restored by substituting the remaining radial integral with a d-dimensional equivalent while ensuring that prefactors reflect the correct surface area of the hypersphere in d dimensions. This procedure ensures that the constants will be correct in three dimensions, but may differ when another method for the angular integration is chosen. This is not relevant to the general existence of the LAB fixed point. Formally, the replacement rule is

$$\int \frac{d^d k}{(2\pi)^d} f(\vec{k}) \longrightarrow \int \frac{dk}{(2\pi)^d} \int d\Omega(\theta,\phi) f(\vec{k}) \longrightarrow \int \frac{dk^d}{(2\pi)^d} S_3^{-1} F(|\vec{k}|) \qquad (21)$$
$$F(|\vec{k}|) \coloneqq \int d\Omega(\theta,\phi) f(\vec{k}).$$

Here, S_d signifies the surface area of the unit hypersphere in d dimensions, in particular $S_3 = 4\pi$ and $S_4 = 2\pi^2$. It is easy to check that this procedure produces the correct result for an isotropic integrand.

Since in (20), the angular and radial dependence of the integrand separate, it follows

$$\Sigma_\varphi(\vec{q}, 0) = -8\pi m e^2 \mu^\epsilon S_3^{-1} \int \frac{d^d k}{(2\pi)^d} \frac{1}{k^4} \times q^2 \qquad (22)$$

As it should be, the integral shows a logarithmic divergence in $d = 4$ and has am ϵ-peak $\sim 1/\epsilon$ in $d < 4$.

For the general case, we briefly sketch the important parts of the calculation. The particle-hole asymmetry y does influence the location of the poles, but changes neither the value of the residues nor the sign of an eigenenergy (moving it between the half planes). Therefore, the final result only depends on x. After the expansion in q and the resolution of the frequency integration, the integrand does separate again in an angular and a radial part where the angular part depends on x. It has no longer an analytic solution, but can be encoded in an *anisotropy function* $f_3(x)$ (the notation follows Moon et al. here). The explicit form is complex and is given in appendix C – we present is the asymptotic form here [2]. The integral can then be treated numerically which leads to the function displayed in figure 3.

$$f_3(x) = -\frac{3}{8\pi}\int d\Omega_k \frac{x^4 \hat{k_x}^2 \left(\hat{k_y}^2 - \hat{k_z}^2\right)^2}{\left(\sqrt{1+x(2+x)p_c(\hat{k})}\right)^5} + \mathcal{O}\left(\frac{1}{x}\right) \tag{23}$$

It is $f_3(0) = 1$ for the isotropic system and $f_3(x \to \infty) \approx 0.88$. Thus, the bosonic self energy at one-loop level becomes

$$\Sigma_\varphi(\vec{q}, 0) = 8\pi m e^2 \mu^\epsilon f_3(x) S_3^{-1} \int \frac{d^d k}{(2\pi)^d} \frac{1}{k^4} \times q^2. \tag{24}$$

This result still contains the arbitrary momentum scale μ and an IR divergence that needs to be taken care off with a lower momentum cutoff a. Near $d = 4$, both dependencies vanish since $\int d^d k k^{-4} \sim a^{-\epsilon}/\epsilon$ which equals $1/\epsilon$ in the limit $\epsilon \to 0$. Similarly, the unphysical momentum scale dependence vanishes since $\mu^\epsilon \to 1$. When keeping track of all factors arising from the angular integration, it is

$$\mu^\epsilon S_3^{-1} \int \frac{d^d k}{(2\pi)^d} \frac{1}{k^4} = \frac{1}{\epsilon} \frac{S_d}{S_3 (2\pi)^d} = \frac{1}{\epsilon} \frac{1}{32\pi^3}. \tag{25}$$

The last equality is valid in $d = 4$ ($\Leftrightarrow \epsilon = 0$). From here on, we can directly insert this concrete value whenever the corresponding integral appears. The final result for Σ_φ reads

$$\Sigma_\varphi(\vec{q}, 0) = \frac{m e^2 f_3(x)}{4\pi^2 \epsilon} q^2. \tag{26}$$

2.3.2. Fermionic Self Energy and Vertex Correction

Let's turn to the fermionic self energy. The calculations proceed in analogy to the bosonic ones, with the minor complication that the fermionic self energy is a 4×4 matrix. It breaks down in three independent coefficients, one associated with the unity matrix and two with the distinct subsets of gamma matrices (index $1, 2, 3$ and $4, 5$). These coefficients will be denoted by F_0, F_1 and F_2, respectively. For the same reasons as for the bosonic part, the first order contribution vanishes. The constant part contains no ϵ-peak and can therefore be neglected for the dimensional

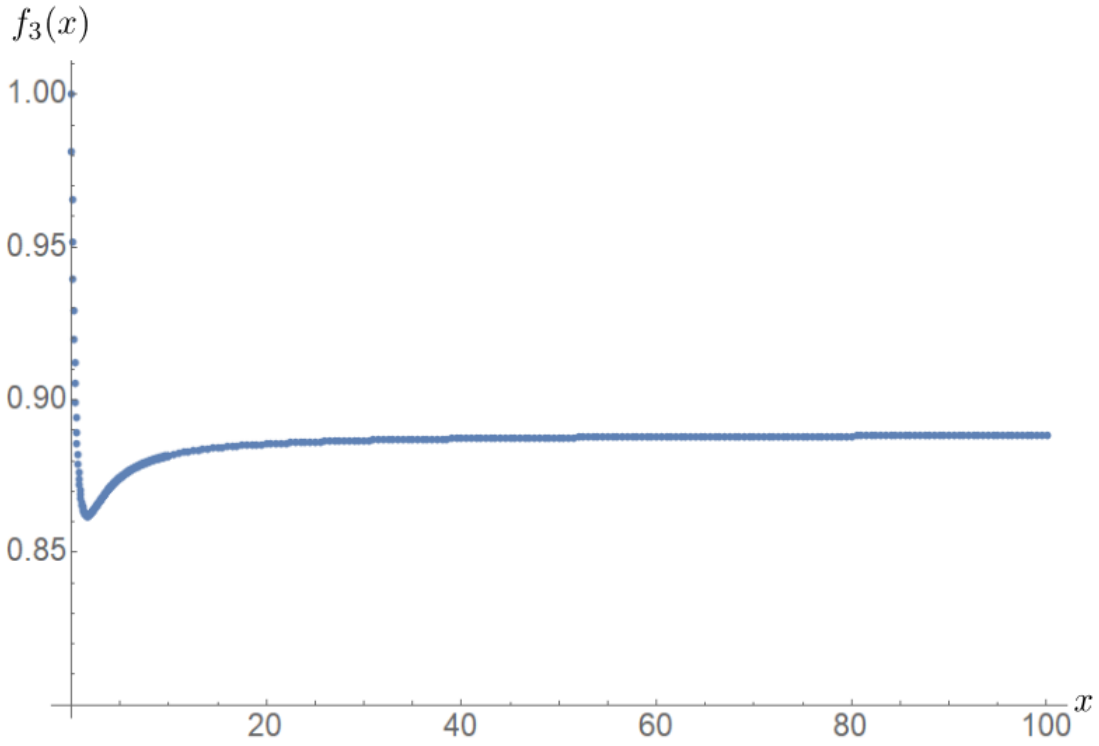

Figure 3: The anisotropy function $f_3(x)$ for the bosonic self energy. It is normalized to 1 for the isotropic system and converges towards a value of about 0.88 for strong anisotropy.

regularization. The second order part is given by

$$\Sigma_f^{(2)}(\vec{q},\omega) = F_0 q^2 \mathbb{1} + F_1 \sum_{a=1}^{3} \Gamma_a d_a(q) + F_2 \sum_{a=4}^{5} \Gamma_a d_a(q). \tag{27}$$

$$\begin{aligned} F_0 q^2 &= \frac{1}{4}\mathrm{Tr}(\Sigma_f^{(2)}) \\ F_1 d_1(q) &= \frac{1}{4}\mathrm{Tr}(\Sigma_f^{(2)}\Gamma_1) \\ F_2 d_4(q) &= \frac{1}{4}\mathrm{Tr}(\Sigma_f^{(2)}\Gamma_4). \end{aligned} \tag{28}$$

It will be seen shortly that the form of the matrix components indeed results in the Γ_a contribution being proportional to $d_a(q)$. The fermionic self energy is independent of the external frequency because the bosonic Green's function is. A

momentum shift therefore cancels its apparent dependence. The one-loop diagram is given by

$$\Sigma_f(\vec{q},\omega) = -e^2\mu^\epsilon \int \frac{d^dk}{(2\pi)^d} \int \frac{d\omega}{2\pi}\, G_f(\vec{k}, i\omega) G_\varphi(\vec{k}+\vec{q}, i(\omega+\Omega)). \tag{29}$$

Let's now turn to the three contributions in (27). For F_0, plugging in the Green's functions yields

$$F_0 q^2 = -2me^2\mu^\epsilon \int \frac{d^dk}{(2\pi)^d} \int \frac{d\omega}{2\pi}\, \frac{4\pi}{(\vec{k}+\vec{q})^2} \cdot \frac{(-2mi\omega + yk^2)}{(-2mi\omega+yk^2)^2 - k^4 - x(2+x)p_c(k)}. \tag{30}$$

On the right-hand side, expansion to second order in q is understood from here on. The right fraction has the form $(z^2-a^2)/((z-a)^2-b^2)$ with a and b depending on k. The residues at its poles however are independent of a and b such that the integral becomes independent of the external momentum q. Therefore, there is no second-order contribution and $F_0 = 0$. It is to note that there is an (infinite) constant term that can be absorbed by a global shift of the energy. For this reason, it will be dropped.

The information relevant to the dimensional regularization procedure is contained in the F_1 and F_4 part.

$$F_1 d_1(q) = -2me^2\mu^\epsilon \int \frac{d^dk}{(2\pi)^d} \int \frac{d\omega}{2\pi}\, \frac{4\pi}{(\vec{k}+\vec{q})^2} \cdot \frac{d_1(k)}{(-2mi\omega+yk^2)^2 - k^4 - x(2+x)p_c(k)} \tag{31}$$

As the boson propagator is frequency-independent, the frequency integration and expansion in q can be performed simultaneously. The integrand contains two poles, one in each half plane. The contour can again be closed in either one, resulting in one pole contributing to the integral. It is

$$\mathrm{Res}\left(\frac{1}{z^2-a^2}, z=a\right) = \frac{1}{2a} \tag{32}$$

$$\partial_{q_i}\partial_{q_j}\left.\frac{1}{(\vec{k}+\vec{q})^2}\right|_{q=0} = \frac{8k_ik_j}{k^6} \quad (i \neq j). \tag{33}$$

It is clear that the k-integral vanishes by antisymmetry unless i and j in (33) match the components in $d_1(k) = -\sqrt{3}k_yk_z$. The second-order contribution F_1 reads therefore

$$F_1 = -16\pi e^2\mu^\epsilon \int \frac{d^dk}{(2\pi)^d} \frac{k_y^2k_z^2}{k^6\sqrt{k^4+x(2+x)p_c(k)}}. \tag{34}$$

Similarly to the bosonic self energy, the angular and radial integrals will be split for the final result

$$\begin{aligned} F_1 &= -8\pi^2(4\pi)e^2\mu^\epsilon S_3^{-1} f_1(x) \int \frac{d^dk}{(2\pi)^d}\frac{1}{k^4} \\ f_1(x) &= \frac{2}{\pi}\int d\Omega_k \frac{\hat{k_y}^2\hat{k_z}^2}{\sqrt{1+x(2+x)p_c(\hat{k})}}. \end{aligned} \tag{35}$$

Again, $\hat{k}$ denotes the unit vector in $\vec{k}$ direction. $f_1(x)$ will be displayed together with $f_2(x)$ from the upcoming calculation in figure 4.

Finally, the computation of F_4 proceeds in the same way:

$$F_4 d_4(q) = -2me^2\mu^\epsilon(1+x)\int\frac{d^dk}{(2\pi)^d}\int\frac{d\omega}{2\pi}\,\frac{4\pi}{(\vec{k}+\vec{q})^2}\cdot\frac{d_4(k)}{(-2mi\omega+yk^2)^2-k^4-x(2+x)p_c(k)} \tag{36}$$

The form of d_4 makes the expansion in q slightly more delicate. It is

$$(\partial_{q_i})^2\left.\frac{1}{(\vec{k}+\vec{q})^2}\right|_{q=0} = \frac{8k_i^2}{k^6} - \frac{2}{k^4}. \tag{37}$$

Because d_4 is antisymmetric under exchange of k_x and k_y, the only contribution

comes from the first addend. For the same reason, the q_z^2 term vanishes. After the frequency integration has been resolved with the residue theorem, it is

$$\begin{aligned} F_4 d_4(q) &= -16\pi e^2 \mu^\epsilon (1+x) \int \frac{d^d k}{(2\pi)^d} \frac{\frac{-\sqrt{3}}{2}(k_x^2 - k_y^2)(k_x^2 q_x^2 + k_y^2 q_y^2)}{k^6 \sqrt{k^4 + x(2+x)p_c(k)}} \\ &= -8\pi e^2 \mu^\epsilon (1+x) \int \frac{d^d k}{(2\pi)^d} \frac{(k_x^2 - k_y^2)^2}{k^6 \sqrt{k^4 + x(2+x)p_c(k)}} \times d_4(q). \end{aligned} \tag{38}$$

The last equality follows by splitting the integral to separate the addends of the second factor, then exchanging k_x and k_y under the second integral and recombining. The final result is

$$\begin{aligned} F_4 &= -8\pi^2 e^2 \mu^\epsilon S_3^{-1} f_2(x)(1+x) \int \frac{d^d k}{(2\pi)^d} \frac{1}{k^4} \\ f_2(x) &= \frac{1}{\pi} \int d\Omega_k \frac{\left(\hat{k_x}^2 - \hat{k_y}^2\right)^2}{\sqrt{1 + x(2+x)p_c(\hat{k})}}. \end{aligned} \tag{39}$$

The anisotropy functions $f_1(x)$ and $f_2(x)$ are shown in figure 4. Both have $f_{1/2}(0) = \frac{8}{15}$ and $f_{1/2}(x \to \infty) = 0$ in common.

Finally, the computation of the vertex correction is not needed explicitly. The frequency independence of the fermionic self energy at one-loop level ensures that it vanishes due to a Ward identity. For a brief derivation of this fact, see appendix B. At higher orders, the self energy will depend on the external frequency and a vertex correction will appear naturally [2].

2.4. Dimensional Regularization and Flow Equations

We proceed now with the renormalization procedure. Taking into account the nonzero contributions of the one-loop diagrams (24), (35) and (39), three Z-factors Z_3, Z_1 and Z_2 need to be introduced to eliminate the first-order divergences in ϵ:

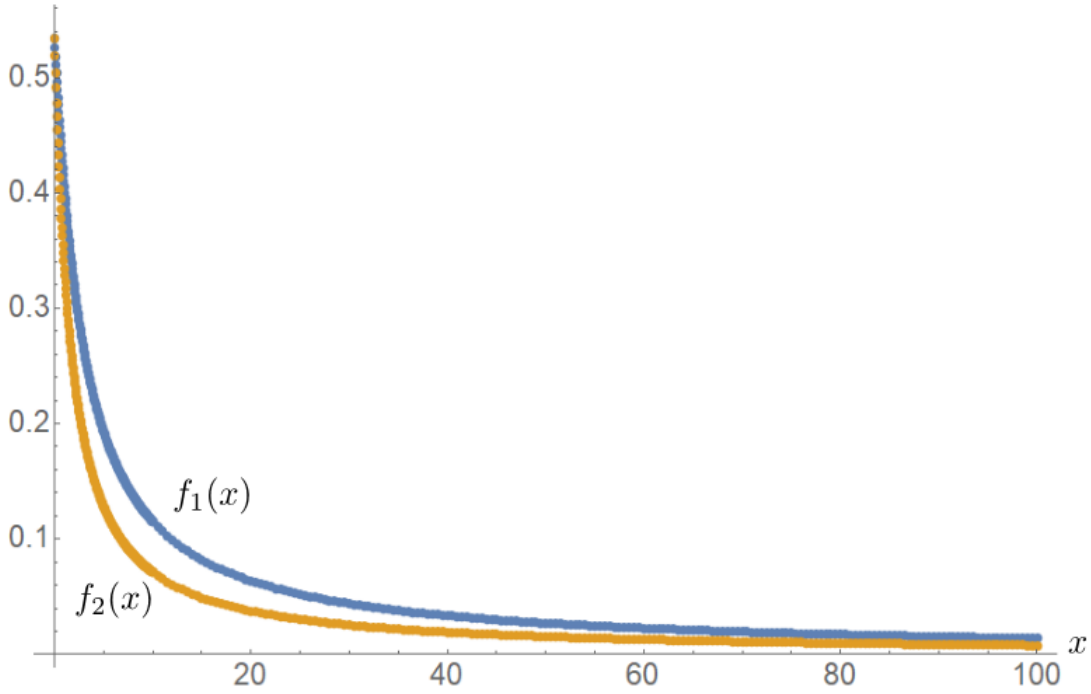

Figure 4: The anisotropy functions $f_1(x)$ and $f_2(x)$ for the fermionic self energy.

$$
\begin{aligned}
S = \int_q \sum_\omega \Psi^\dagger(q,i\omega)\left(-i\omega + \frac{q^2}{2M_0} + Z_1 \sum_{a=1}^{3} \frac{d_a(q)\Gamma^a}{2m} + Z_2 \sum_{a=4}^{5} d_a(q)\Gamma^a \left(\frac{1}{2m} + \frac{1}{2M_c}\right)\right)\Psi(q,i\omega) \\
- ie\mu^{\frac{\epsilon}{2}} \int_{q,k} \sum_{\omega,\Omega} \Psi^\dagger(q+k, i\omega + i\Omega)\varphi(k,i\Omega)\Psi(q,i\omega) \\
+ \frac{1}{8\pi} Z_3 \int_k \sum_\Omega \varphi(-k,-i\Omega)k^2\varphi(k,i\Omega) \qquad (40)
\end{aligned}
$$

With the results of the previous sections, they take the form

$$
\begin{aligned}
Z_3 &= 1 + \frac{1}{\pi\epsilon} m e^2 f_3(x) \\
Z_1 &= 1 + \frac{1}{2\pi\epsilon} m e^2 f_1(x) \\
Z_4 &= 1 + \frac{1}{2\pi\epsilon} m e^2 f_2(x)(1+x).
\end{aligned}
\tag{41}
$$

Here, the d-dimensional integrals have been resolved according to (25). To restore the original form of the action, rescaling has to be done as given in (42). Quantities with the B subscript represent the bare versions.

$$
\begin{aligned}
\varphi_B &= Z_3^{\frac{1}{2}} \varphi \\
\left(\frac{1}{m}\right)_B &= Z_1 \frac{1}{m} \\
\left(\frac{1}{m}(1+x)\right)_B &= Z_4 \left(\frac{1}{m}(1+x)\right) \\
e_B &= \mu^{-\frac{\epsilon}{2}} Z_3^{-\frac{1}{2}} e
\end{aligned}
\tag{42}
$$

All other quantities don't acquire anomalous dimensions. Introducing a dimensionless coupling $u \coloneqq me^2/2\pi$, the β-functions ($\beta_\xi \coloneqq \mu \frac{d\xi}{d\mu}$) become

$$
\begin{aligned}
\beta_{\frac{1}{m}} &= (z-2)\frac{1}{m} + u f_1(x) \frac{1}{m} \\
\beta_y &= -u f_1(x) y \\
\beta_x &= -u(1+x)(f_1(x) - f_4(x)) \\
\beta_u &= \epsilon u - (2 f_3(x) + f_1(x)) u^2.
\end{aligned}
\tag{43}
$$

The equation for the interaction strength u has a fixed point at a finite value u_c:

$$
u_c = \frac{\epsilon}{2 f_3(x) + f_1(x)} \underset{x=y=0}{=} \frac{15}{38}\epsilon \tag{44}
$$

Since $u_c > 0$, both mass ratios x and y are irrelevant there. Furthermore, the

fixed point is stable. To keep m (and thus the energy scale) fixed, one can choose $z = 2 - f_1(x)u$ which results in the dynamical critical exponent $z = 2 - 4\epsilon/19$ at the fixed point. This is the isotropic, stable LAB fixed point.

2.5. The LAB Phase and Further Results

To conclude the section on the LAB phase, the key characteristics of the LAB fixed point relevant for this thesis will be presented alongside some further research results.

We don't treat any experimental indicators for a LAB phase here, but concentrate on the theoretical fixed point and the implications of finite temperature. Moon et al. give a way of calculating the scaling of any operator and hence physical observable [2]. They explicitly do so for some thermodynamic response functions such as the specific heat $c_v \sim T^{1.7}$ and spin susceptibility $\chi \sim a + bT^{0.5}$. Their results for the electric conductivity leads to (undoped) LAB materials being power-law insulators. Additionally, they perturbatively analyze the effect of a strain δ and a Zeeman field H and arrive at multiple phases in the δ-H parameter plane. These results are of no particular interest for the computations of this thesis, but of course relevant to the actual detection of the LAB phase.

Additional research around the Luttinger Hamiltonian and the LAB phase has been conducted by Igor Herbut and his group [9][10]. The most important result is the treatment of possible phases adjacent to the LAB to arrive – at least qualitatively – at a phase diagram with possible temperature boundaries on the appearing of the LAB phase. They include additional couplings $g_1(\Psi^\dagger\Psi)^2$ and $g_2(\Psi^\dagger\Gamma_a\Psi)^2$ in the action leading to a new quantum critical point at $g_1, g_2 \neq 0$ which with increasing ϵ collides with the LAB fixed point at a lower critical dimension $d_{low} \approx 3.26$ and leaves only a runaway flow in the parameter space at lower dimension. They argue that the LAB scaling remains observable in a certain temperature window $[T_c, T^*]$ where at T_c, the system undergoes a phase transition towards a gapped Mott insulator ground state and T^* is a crossover temperature to the usual Fermi liquid phase. The estimates are based on a comparison of typical thermal and LAB length scales.

Furthermore, Igor Boettcher and Igor Herbut [11] argue that despite the isotropic

nature of the LAB fixed point, the RG flow of the anisotropy x (or an equivalent parameter) is exceptionally slow such that it can be treated as approximately constant during the RG flow. They come to the conclusion that in this setting, anisotropy actually supports the formation of the LAB phase by making it observable in a wider range of temperatures and lowering the lower critical dimension d_{low} discussed above.

3. Screened Potential Approach

As a first estimate of the influence of temperature on the LAB phase, we explore a screening length approach: the unscreened Coulomb interaction that results in the zero-temperature LAB phase will be replaced by a screened version with a Yukawa-like decay $\sim e^{-x/l_{scr}}/x$. The screening length l_{scr} can be estimated based on the bosonic self energy at absolute zero as described in the following section. This is the essence of the random phase approximation (RPA), capturing the effects of interaction in a screened potential. Igor Herbut and Lukas Janssen [9] have identified a characteristic length scale for the LAB phase l_{LAB} in three dimensions which will be compared against l_{scr}. If the screening length is much smaller than the LAB characteristic length, the LAB phase is expected to be severely affected – possibly destroyed or altered – because the Coulomb interaction is already thermally suppressed over the relevant length scales. In the opposite case, screening only kicks in at a greater length scale and the non-Fermi liquid behavior should be observable without drastic changes. However, the scope of this section lies in searching qualitative evidence since a naive screening approach cannot be expected to yield quantitative results in terms of the observability of the LAB phase.

3.1. Calculation of the Screening Length

This section will briefly explain the link between the bosonic self energy and screening length following [12, p.223-225] and then turn to deriving an expression for the latter. In the self energy approach, the bosonic Green's function G_φ is the solution of a Dyson equation:

$$G_\varphi(\vec{k}) = G_0(\vec{k}) + G_0(\vec{k})\Sigma_\varphi(\vec{k})G_\varphi(\vec{k}) \tag{45}$$

Here, G_0 denotes the noninteracting Green's function. A formal solution is given by

$$G_\varphi^{-1} = G_0^{-1} - \Sigma_\varphi^{-1}. \tag{46}$$

Plugging in the free bosonic Green's function $4\pi/k^2$ and using that all quantities are scalar in our case yields

$$G_\varphi(\vec{k}) = \frac{4\pi}{k^2 - 4\pi\Sigma_\varphi(\vec{k})}. \tag{47}$$

Neglecting all but the constant part of the self energy $\Sigma_\varphi(0)$ and applying a Fourier transform to the three-dimensional position space results in a Yukawa-like Green's function describing the screened Coulomb interaction. The characteristic screening length is given by $l_{scr} \coloneqq (-4\pi\Sigma_\varphi(0))^{-\frac{1}{2}}$.

$$G_\varphi(\vec{r}) = \frac{e^{-\frac{r}{l_{scr}}}}{r} \tag{48}$$

Let's now turn to the computation of the constant part of the bosonic self energy. This is the first calculation carried out at finite temperature: this corresponds to replacing the frequency integrals from the previous section by Matsubara sums. The use of an artificial length scale μ is not necessary in this section as we fix $d = 3$. To avoid confusion with the other chapters, the physical interaction constant – which we avoided to use in dimensional regularization because it changes units with varying ϵ – shall be denoted by $\tilde{e}$. It is related to the previously used one by $\tilde{e}^2 = e^2\mu^\epsilon$, in particular $\tilde{e}^2 = e^2\mu$ in three dimensions. The integral to solve is given by

$$\Sigma_\varphi(0) = -\tilde{e}^2 \int \frac{d^3k}{(2\pi)^3} \sum_{\omega_n} \mathrm{Tr}\left\{G_f(\vec{k}, i\omega_n)^2\right\} \tag{49}$$

$$= -4(2m)^2\tilde{e}^2 \int \frac{d^dk}{(2\pi)^d} \frac{1}{\beta} \sum_{\omega_n} \frac{(-2mi\omega_n + yk^2)^2 + k^4 + x(2+x)p_c(k)}{[(-2mi\omega_n + yk^2)^2 - k^4 - x(2+x)p_c(k)]^2}. \tag{50}$$

The frequency sum runs over fermionic Matsubara frequencies $\omega_n \coloneqq (2n+1)\pi/\beta$ with inverse temperature β and will be evaluated by transforming it into an integral over $z \coloneqq 2mi\omega$ with an additional fermionic occupation function $n_F(z/2m))$ under the integral. This method to resolve Matsubara sums is briefly recapitulated in appendix A. The final path derived there is $\mathcal{C}_3$ enclosing all but the imaginary axis of the complex z space – this means that the poles of $n_F(z)$ located at $2mi\omega_n$

don't contribute. Unless otherwise noted, all complex contour integrals from here on are to be taken along $\mathcal{C}_3$.

$$\Sigma_\varphi(0) = -8m\tilde{e}^2 \int \frac{d^3k}{(2\pi)^3} \oint \frac{dz}{2\pi} n_F\left(\frac{z}{2m}\right) \frac{(-z+yk^2)^2 + k^4 + x(2+x)p_c(k)}{[(-z+yk^2)^2 - k^4 - x(2+x)p_c(k)]^2} \tag{51}$$

$$n_F(z) \coloneqq \frac{1}{e^{\beta z}+1} \tag{52}$$

The z integral is solved with the aid of the residue theorem, it is

$$\mathrm{Res}\left[(\text{integrand of (51)}), z = 2mE_\pm\right] = \frac{-\beta}{4m} \frac{e^{\beta E\pm}}{(1+e^{\beta E_\pm})^2}. \tag{53}$$

We recall that $E_\pm$ denote the eigenenergies of the Hamiltonian. Summing up the residues leads to

$$\Sigma_\varphi(0) = -2\tilde{e}^2\beta \int \frac{d^3k}{(2\pi)^3} \frac{1+\cosh\left(\frac{y\beta k^2}{2m}\right)\cosh\left(\frac{\beta}{2m}\sqrt{k^4 - x(2+x)p_c(k)}\right)}{\left[\cosh\left(\frac{y\beta k^2}{2m}\right) + \cosh\left(\frac{\beta}{2m}\sqrt{k^4 - x(2+x)p_c(k)}\right)\right]^2}. \tag{54}$$

The temperature and mass dependence can then be isolated in front of the integral by passing to spherical coordinates and substituting $k^2 \to \beta k^2/(2m)$.

$$\Sigma_\varphi(0) = -2(2m)^{\frac{3}{2}}\tilde{e}^2\beta^{-\frac{1}{2}} \int \frac{d^3k}{(2\pi)^3} \frac{1+\cosh(yk^2)\cosh(k^2\sqrt{1 - x(2+x)p_c(\hat{k})})}{\left[\cosh(yk^2) + \cosh\left(k^2\sqrt{1 - x(2+x)p_c(\hat{k})}\right)\right]^2} \tag{55}$$

The momentum integral has no analytic solution, but can easily be solved numerically. For the isotropic, particle-hole symmetric case of $x = y = 0$, it results in

$$\Sigma_\varphi(0) \approx 0.15 m^{\frac{3}{2}} \tilde{e}^2 \beta^{-\frac{1}{2}} \tag{56}$$

$$l_{scr} \approx 0.72 \frac{\beta^{\frac{1}{4}}}{m^{\frac{3}{4}} \tilde{e}}. \tag{57}$$

This result agrees with Ipsita Mandal [13] who calculated the screening length in the same system for the isotropic Hamiltonian.

Finally, let's turn to the influence of x and y. For efficiency, the numerical integration has been performed with a Monte Carlo method to a precision sufficient to see general tendencies – maximum accuracy was not the goal. The displayed "jumps" in some of the quantities are not expected to be physical, but numerical artifacts because Σ_φ is small.

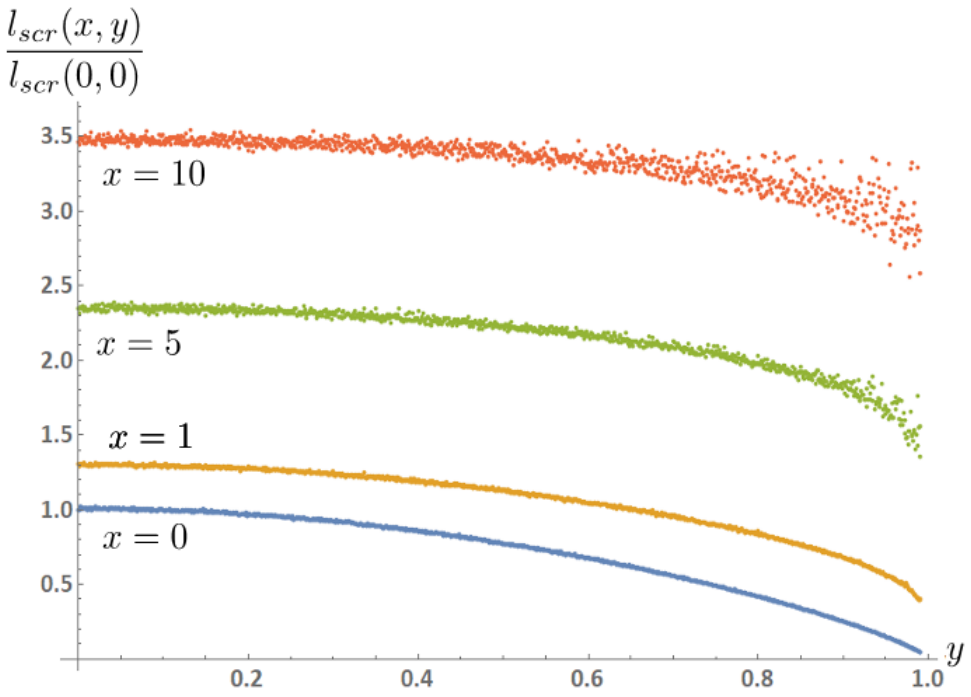

Figure 5: Dependence of the screening length on the particle-hole asymmetry y for selected values of x. The noise for higher x is a numerical artifact due to the decreasing self energy close to zero.

Figure 5 shows that the y-dependence is not dominant and gets even weaker when $x \neq 0$. It is to be noted again that $y = 1$ is not a physical value because it leads to a "degenerate" dispersion without a quadratic band touching point – this may be an explanation for the erratic behavior in the vicinity of this limit. We will focus on the $y \ll 1$ case in which y can be comfortably set to zero. There is a slight tendency though for particle-hole-asymmetry to decrease the range of the Coulomb interaction. An intuitive explanation for this phenomenon is that with increasing y, the effective band mass for the negative branches increases while it decreases for the positive ones. This results in a higher density of states for negative energies and vice-versa. Fewer available (empty) states above zero in comparison with the occupied ones below then hinder the interaction.

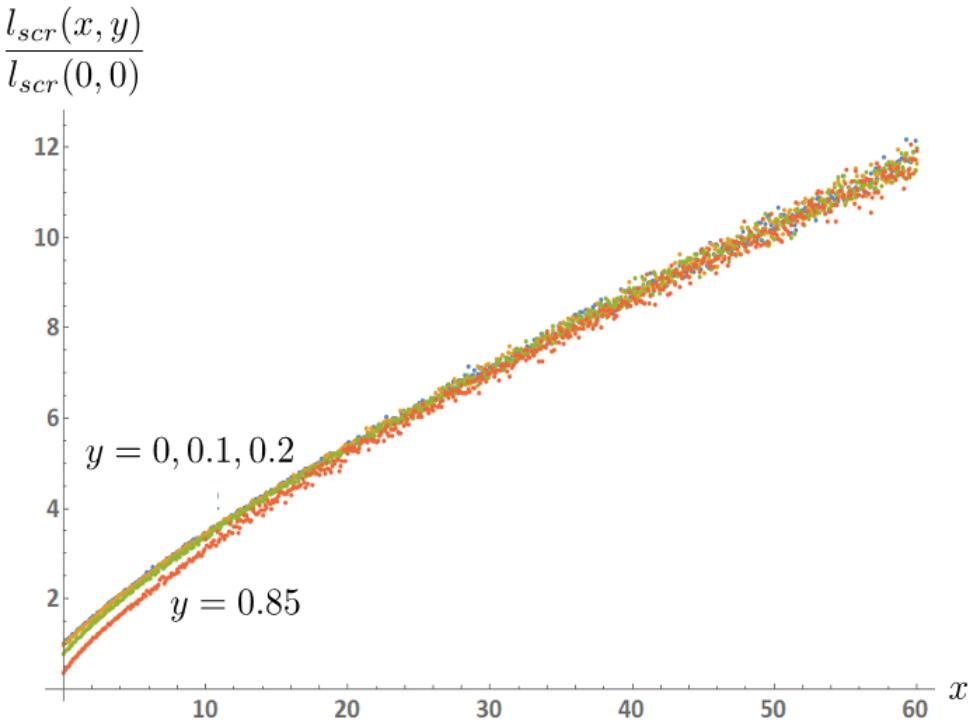

Figure 6: Dependence of the screening length on the anisotropy x for various y.

Figure 6 clearly shows that the anisotropy is a more relevant parameter when it comes to the screening length. For the most part, the screening length seems to scale linearly in x, with a slightly stronger screening for small x. Anisotropy

therefore reduces the importance of screening in the finite temperature case – this translates into supporting the formation of a LAB-like phase at finite temperature. This result is in agreement with Boettcher and Herbut finding that anisotropy tends to help the LAB phase [11].

3.2. LAB Length Scale and Comparison

The LAB phase emerges due to the q^2-contribution in the bosonic and fermionic self energies as seen in sections 2.3.1 and 2.3.2. Specifically, the form of the Z-factors in (41) results in the flow equations and determines the strength of the flow. In $d = 3$ ($\epsilon = 1$), the characteristic length scale l_{LAB} is given by

$$l_{LAB} = \frac{1}{8\pi m \tilde{e}^2 f_3(x)}. \tag{58}$$

This is to be seen as an order of magnitude – here, l_{LAB} is chosen as the point where $Z_0 = 2$. Below this scale, the non-Fermi liquid behavior can be observed – or put differently, LAB electrons are strongly correlated over this scale. It corresponds to the one Herbut et al. identify for the NFL behavior to set in and that they use to estimate a transition temperature by comparing it to the inverse of a characteristic thermal momentum [9].

For simplicity, let's start with the isotropic case $x = 0$ where $f_3(x) = 1$ and the screening length is given by (56). Due to the overall weak dependence on y, the particle-hole asymmetry will be set to zero as well. The ratio of the two relevant length scales is given by

$$K := \frac{l_{scr}}{l_{LAB}} = 12.1(\beta m)^{\frac{1}{4}} \tilde{e}. \tag{59}$$

As a consistency check, this quantity is indeed dimensionless: in natural units, β is an inverse energy while m is an energy and $\tilde{e}$ is dimensionless (as $\tilde{e}^2/r$ is the Coulomb energy). Now, $K \ll 1$ means that screening interferes critically with the LAB phase by modifying the Coulomb interaction over the relevant length scales. $K \gg 1$ is the opposite case of screening having little influence. Naturally, K decreases with rising temperature, but the exponent $\frac{1}{4}$ constitutes a rather weak dependence. Unsurprisingly, a stronger interaction $\tilde{e}$ helps the LAB phase survive,

as does an increase of the symmetric band mass m.

Now, let's find sensible values for β, m and $\tilde{e}$. It is easiest to remain in natural units. According to Herbut et al., temperatures relevant to the LAB phase are of the order $10 \ldots 100\,\mathrm{K}$ [9] which yields inverse thermal energies $\beta \approx 0.1 \ldots 1\,\mathrm{meV}^{-1}$. Relative band masses (compared with the free electron mass) range from 0.02 to about 1 and translate into $m \approx 10 \ldots 500\,\mathrm{keV}$. The dimensionless coupling $\tilde{e}$ is obtained by combining the fine structure constant $\alpha = \tilde{e}^2/4\pi \approx 1/137$ with an estimate for the relative permittivity which will be taken between 1 and 30 here. Altogether, this results in $\tilde{e} \approx 0.3 \ldots 1.66$. The overall ratio K is mainly driven by the fraction of electron band mass and thermal energy which is in the order of magnitude 10^6. The prefactors together with the fourth root then result in $K \sim 10^2 \ldots 10^3 \gg 1$. In the RPA approximation, screening should have no drastic impact on the LAB phase. As shown in figure 7, the temperature dependence $\sim T^{-\frac{1}{4}}$ is weak enough such that this holds over a large range.

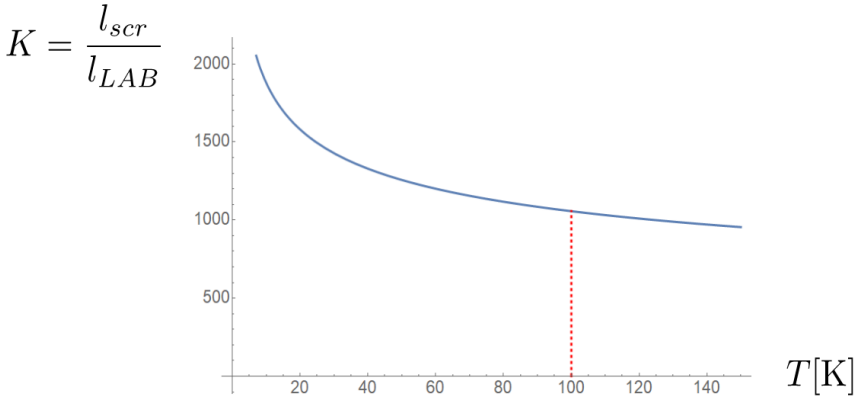

Figure 7: K over T for $\tilde{e} = 1$ and $m = m_{el}$. The weak dependence on T ensures that $K \gg 1$ for the whole temperature range in question up to 100Kelvin, marked by the red dashed line.

Including anisotropy in the calculation will assist the LAB phase by weakening the screening even more as shown in figure 6. l_{LAB} stays relatively unchanged due to $f_3(x) = \mathcal{O}(1)$ for all x. At extreme values of the particle-hole asymmetry $y \lesssim 1$, screening will take over, but this should be attributed to the general breakdown of the dispersion for $y \to 1$. For reasonable values of y, there should be no drastic change.

4. Dimensional Regularization at Finite Temperatures

Let's now turn to a more rigorous approach. The goal of this section is to retrace the renormalization calculation which leads to the LAB phase for the case of nonzero temperature. This corresponds again to the replacement of frequency integrals with Matsubara sums which will then be solved by introducing fermionic occupation functions $\sim (e^{\beta z}+1)^{-1}$. At the very least, temperature is expected to be a relevant parameter which manifests as a runaway flow in the phase space and thus renders the LAB fixed point unstable

4.1. Self Energies

As for the zero temperature case, the first step towards the flow equations is deriving an expression for the various one-loop-diagrams and examining their temperature dependency.

4.1.1. Bosonic Self Energy

The starting point for the bosonic self energy reads

$$\Sigma_\varphi(\vec{q},\Omega) = -e^2\mu^\epsilon \int \frac{d^dk}{(2\pi)^d}\frac{1}{\beta}\sum_{\omega_n} \mathrm{Tr}\left\{G_f(\vec{k},i\omega)G_f(\vec{k}+\vec{q},i\omega+i\Omega)\right\} \tag{60}$$

where the frequency sum runs over fermionic Matsubara frequencies $\omega_n = (2n+1)\pi/\beta$. For simplicity, the external frequency Ω will again be set to zero. When expanding the integrand in small q, the first order term will vanish due to the asymmetry in k-components. The constant part is in analogy to (55) given by

$$\Sigma_\varphi(0) = -e^2\mu^\epsilon\beta \int \frac{d^dk}{(2\pi)^d}\frac{1+\cosh\left(\frac{y\beta k^2}{2m}\right)\cosh\left(\frac{\beta}{2m}\sqrt{k^4-x(2+x)p_c(k)}\right)}{\left[\cosh(\frac{y\beta k^2}{2m})+\cosh\left(\frac{\beta}{2m}\sqrt{k^4-x(2+x)p_c(k)}\right)\right]^2} \tag{61}$$

in general dimension d. It is no longer zero, but finite for all dimensions d: for small k, the integrand tends to $\frac{1}{2}$ while it vanishes exponentially $\sim e^{E_-(k)}$ for large

k. Therefore, no ϵ-peak appears and no cancellation of infinities and subsequent rescaling is necessary.

Hence, the second order term is therefore the important one for renormalization. The case $x = y = 0$ will be examined first by reusing the results of section 2.3.1. It is

$$\Sigma_\varphi(\vec{q},0) = -16(me)^2\mu^\epsilon \int \frac{d^dk}{(2\pi)^d}\frac{1}{\beta}\sum_{\omega_n}\frac{(2mi\omega)^2 + k^4 + \frac{3\cos^2\theta-1}{2}k^2q^2}{[(2mi\omega)^2 - k^4][(2mi\omega)^2 - (\vec{k}+\vec{q})^4]}. \quad (62)$$

As a next step, the frequency sum is transformed into a contour integral ($\mathcal{C}_3$ understood) by introducing $n_F(z)$ while substituting $z = 2mi\omega$.

$$\Sigma_\varphi(\vec{q},0) = +4me^2\mu^\epsilon \int \frac{d^dk}{(2\pi)^d}\oint \frac{dz}{2\pi i} n_F\left(\frac{z}{2m}\right)\frac{z^2 + k^4 + \frac{3\cos^2\theta-1}{2}k^2q^2}{[z^2 - k^4][z^2 - (\vec{k}+\vec{q})^4]} \quad (63)$$

It is easiest to expand the integrand in small q before resolving the z-integration. Both operations do commute, choosing this order avoids dealing with infinities in q at intermediate steps however (which of course cancel out in the end). The fraction expands to

$$\begin{aligned}\frac{z^2 + k^4 + \frac{3\cos^2\theta-1}{2}k^2q^2}{(z^2 - k^4)(z^2 - (\vec{k}+\vec{q})^4)} &= \frac{z^2 + k^4}{(z^2 - k^4)^2} + \frac{4k^2(z^2 + k^4)}{(z^2 - k^4)^3}(\vec{k}\cdot\vec{q}) \\ &+ \frac{(5 - 27\cos^2\theta)k^4 + (3 - 53\cos^2\theta)z^2}{2(z^2 - k^4)^3}k^2q^2 + \frac{32z^4}{(z^2 - k^4)^4}(\vec{k}\cdot\vec{q})^2. \quad (64)\end{aligned}$$

The constant term leads to (61) while the first order term vanishes during the momentum integration. The second order term with poles at $z = \pm k^2$ leads to

$$\Sigma^{(2)}_\varphi(\vec{q},0) = -3\beta me^2\mu^\epsilon \int \frac{d^dk}{(2\pi)^d}\left[\frac{5\cos^2\theta - 1}{k^4}\tanh\frac{\beta k^2}{4m} + R(k)\right] \times q^2. \quad (65)$$

The rest terms $R(k)$ are of order k^{-2} and exponentially suppressed for large k:

$$R(k) = \frac{(5\cos^2\theta - 1)}{4mk^2\cosh^2\frac{\beta k^2}{4m}} + \frac{(2\cos^2\theta - 1)\beta^2\sinh\frac{\beta k^2}{4m}}{12m^2\cosh^3\frac{\beta k^2}{4m}} + \frac{k^2\beta^3\cos^2\theta\left(2\sinh^2\frac{\beta k^2}{4m} - 1\right)}{32m^3\cosh^4\frac{\beta k^2}{4m}} \tag{66}$$

They represent a finite contribution to the self energy and can be omitted for the dimensional regularization process. After resolving the angular integration with the method described in section 2.3.1, the final result for the isotropic system is

$$\Sigma_\varphi(\vec{q}, 0) = -me^2\mu^\epsilon 8\pi S_d^{-1}\int\frac{d^dk}{(2\pi)^d}\frac{1}{k^4}\tanh\frac{\beta k^2}{4m}\times q^2. \tag{67}$$

Before turning to the fermionic self energy, let's discuss the influence of the parameters x and y. Even with algorithmic assistance, the expansions and residues become quite convoluted which is the reason why a full computation hasn't been made. The starting point is the equation akin to (15). Encouraged by the weak influence of the particle-hole asymmetry y on the screening length, we will leave it at zero. It is worth noting though that it doesn't disappear after the frequency integration anymore – it will instead enter into the fermionic occupation functions and remain inside the hyperbolic functions in the result. The simplified one-loop integral then reads

$$\Sigma_\varphi(\vec{q}, 0) = -16(me)^2\mu^\epsilon\int\frac{d^dk}{(2\pi)^d}\frac{1}{\beta}\sum_{\omega_n}\frac{(2mi\omega)^2 + k^4 + \frac{3\cos^2\theta-1}{2}k^2q^2 + x(2+x)\widetilde{p_c}(k, k+q)}{[(2mi\omega)^2 - \delta_E(k)^2][(2mi\omega)^2 - \delta_E(k+q)^2]} \tag{68}$$

where the auxiliary functions δ_E and $\widetilde{p_c}$ are defined as in section 2.3.1. Transforming the frequency sum into a contour integral and substituting $z = 2mi\omega$ yields

$$\Sigma_\varphi(\vec{q}, 0) = +4me^2\mu^\epsilon\int\frac{d^dk}{(2\pi)^d}\oint\frac{dz}{2\pi i}n_F\left(\frac{z}{2m}\right)\frac{z^2 + k^4 + \frac{3\cos^2\theta-1}{2}k^2q^2 + x(2+x)\widetilde{p_c}(k, k+q)}{[z^2 - \delta_E(k)^2][z^2 - \delta_E(k+q)^2]}. \tag{69}$$

The cubic anisotropy prevents an elegant expansion in q since spherical coordi-

nates are no longer a good basis. Inferring from the isotropic case, the principal symmetries will still lead to only the second-order term in q being relevant for the Z-factors. More than that, the solution will contain a hyperbolic tangent factor similar to (65) with the argument containing the full eigenenergy. This factor then prevents the separation of angular and radial integration. Under these considerations, an educated guess for the relevant part of the bosonic self energy (that is to say, the one containing the ϵ-peak) is given by

$$\Sigma_\varphi(\vec{q},0) = 8\pi m e^2 \mu^\epsilon \int \frac{d^d k}{(2\pi)^d} \frac{1}{k^4} \left[\frac{x^4 \hat{k_x}^2 (\hat{k_y}^2 - \hat{k_z}^2)^2}{\left(\sqrt{1+x(2+x)p_c(\hat{k})}\right)^5} + \mathcal{O}\left(\frac{1}{x^2}\right) \right] \tanh\left(\frac{\beta k^2}{4m}\sqrt{1+x(2+x)p_c(\hat{k})}\right). \quad (70)$$

The part in square brackets is the integrand of $f_3(x)$ in the zero-temperature case – its full form can be found in appendix C. The integral ultimately needs to be solved numerically, though one can factor out the dependency on β and m by substituting $k^2 \to \beta k^2/(4m)$. Then, it depends only on the dimension d and the anisotropy x. For the treatment of the angular integrals, the method described in section 2.3.1 cannot be applied directly – solving the angular portion in 3D is not possible separately from the radial part. However, a variant of this method can be used to extract an anisotropy function $\tilde{f}_3(x)$ analogous to $f_3(x)$: the whole integral including the radial part is computed numerically in three dimensions and the general dimensionality reintroduced artificially to produce the correct ϵ-peak. This procedure is not as rigorous as the separation of angular and radial integrand since the dimension of the k-vector is directly connected with the anisotropy x inside the hyperbolic tangent and can't be strictly separated. However, it allows a much more concrete treatment of the problem in the renormalization group. The resulting anisotropy function is displayed in figure 8.

It may seem problematic to reintroduce an IR divergence this way that is originally suppressed by the temperature factor. However, it is justified because the minimal subtraction of the ϵ-peak doesn't care about finite contributions of the

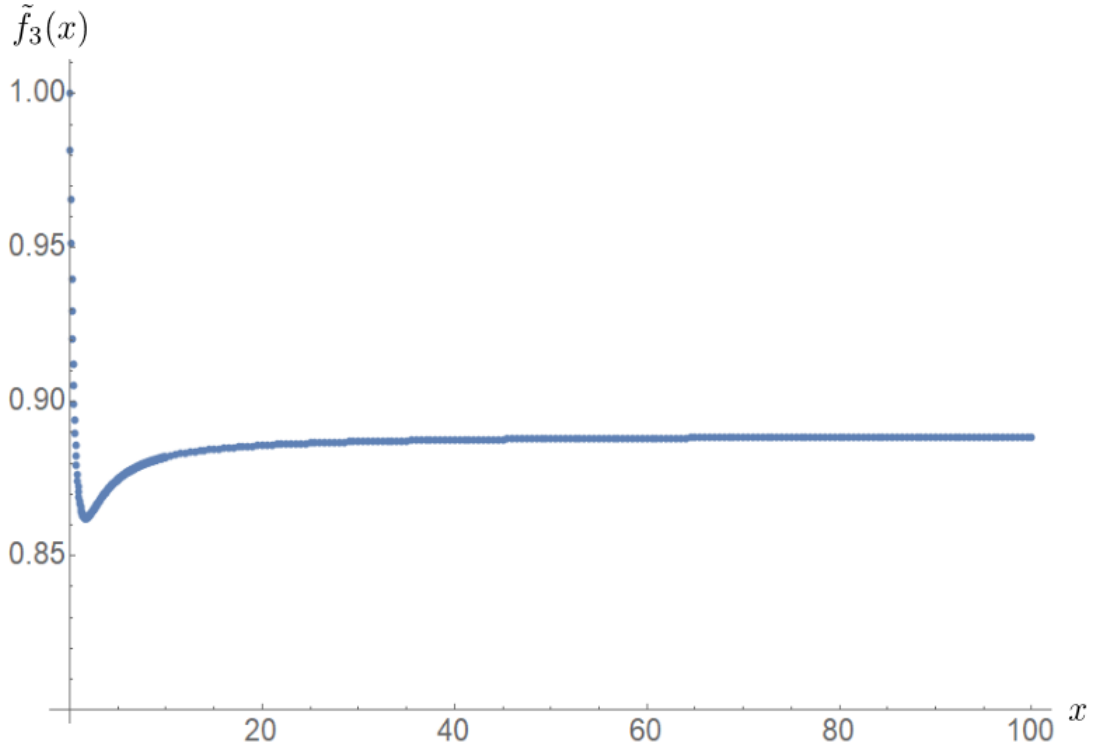

Figure 8: The anisotropy function $\tilde{f}_3(x)$ for the bosonic self energy. It is equal to $f_3(x)$, the zero temperature analogue, when properly normalized to eliminate the unphysical dependency on the arbitrary momentum scale.

self energy, only about the UV divergence when sending $d \to 4$. The dependence on the temperature is a low-momentum phenomenon not related to the ϵ-peak. It can therefore be absorbed into the initially introduced momentum scale μ.

Most importantly, the bosonic self energy acquires a factor that suppresses the integrand at low momenta, but leaves it unchanged at high k. Formally, the integral will assume the form $A/\epsilon + B(T)$ with the temperature contributing to the finite portion. This is because temperature naturally destroys correlation at large length scales while leaving shorter ones relatively untouched. The limit towards zero temperature ($\beta \to \infty$) correctly restores the formerly calculated self energy.

To conclude the discussion of the bosonic self energy, a comment on the striking fact that the anisotropy functions $f_3(x)$ and $\tilde{f}_3(x)$, corresponding to zero and finite temperature, are completely equal. This should surprise when considering that the

hyperbolic tangent factor is strictly smaller than 1: the resolution of this apparent paradox lies in the normalization procedure necessary to ensure independence of μ (because it is an arbitrary scale) and separation of the angular integral. From the "raw" momentum integral $\int d_d k k^{-4}$, the UV components leading to the ϵ-peak need to be extracted while ensuring independence on IR phenomena. This is done by introducing an effective lower cutoff canceling out with the prefactor $\mu^{-\epsilon}$.

4.1.2. Fermionic Self Energy

Let's now pass on to the fermionic self energy. Its components can again be traced out with the Γ matrices and $\mathbb{1}$.

$$\begin{aligned} F_0 &\coloneqq \frac{1}{4}\mathrm{Tr}(\Sigma_f) \\ F_a &\coloneqq \frac{1}{4}\mathrm{Tr}(\Sigma_f \Gamma_a) \end{aligned} \tag{71}$$

At the second order, symmetry will again lead to $F_a \sim d_a(q)$ and an identical form for $a = 1, 2, 3$ and $a = 4, 5$ respectively.

$$\begin{aligned} \Sigma_f(\vec{q}, \Omega) &= -e^2 \mu^\epsilon \int \frac{d^d k}{(2\pi)^d} \frac{1}{\beta} \sum_{\omega_n} G_f(\vec{k}, i\omega) G_\phi(\vec{k} + \vec{q}, i(\omega + \Omega)) \\ &= +e^2 \mu^\epsilon \int \frac{d^d k}{(2\pi)^d} \oint \frac{dz}{2\pi i} n_F\left(\frac{z}{2m}\right) \frac{4\pi}{(\vec{k} + \vec{q})^2} \cdot \frac{-z + yk^2 - d_a(k)\Gamma^a - x(d_4(k)\Gamma^4 + d_5(k)\Gamma^5)}{(z - yk^2)^2 - k^4 - x(2+x)p_c(k)} \end{aligned} \tag{72}$$

Here, the ω_n in the first line are again fermionic and $z = 2mi\omega$ has been substituted in the second line. As for zero temperature, there is no dependence on the external frequency Ω because it doesn't appear in the boson propagator. For that reason, the z integration can be resolved separately. The contour again encloses the poles located at the eigenenergies $z_\pm = 2m(E_0 \pm \Delta_E) = e_0 \pm \delta_E$. Let furthermore $A \coloneqq d_a(k)\Gamma^a + x(d_4(k)\Gamma^4 + d_5(k)\Gamma^5)$ be the sum of the Γ_a-components of the numerator. It is

$$\begin{aligned}
&\oint \frac{dz}{2\pi i} n_F\left(\frac{z}{2m}\right) \frac{-z + e_0 - d_a(k)\Gamma^a - x(d_4(k)\Gamma^4 + d_5(k)\Gamma^5)}{(z-e_0)^2 - (\delta_E)^2} \\
&\quad = -\left(n_F(E_0+\Delta_E)\frac{A+\delta_E}{2\delta_E} - n_F(E_0-\delta_E)\frac{A-\delta_E}{2\delta_E}\right) \\
&\quad = \frac{A}{2\delta_E}\frac{\sinh\beta\Delta_E}{\cosh\beta E_0 + \cosh\beta\Delta_E} + \frac{1}{2}\left(1 - \frac{\sinh\beta E_0}{\cosh\beta E_0 + \cosh\beta\Delta_E}\right).
\end{aligned} \tag{73}$$

This is now plugged back into the self energy and the various components proportional to $\mathbb{1}$ and the Γ_a are computed separately. First, let's focus on the constant part $\Sigma_f(0)$.

$$\begin{aligned}
\Sigma_f(0) = +4\pi e^2\mu^\epsilon \int \frac{d^dk}{(2\pi)^d} \oint \frac{dz}{2\pi i}\frac{1}{k^2}\Bigg[&\frac{A}{2\delta_E}\frac{\sinh\beta\Delta_E}{\cosh\beta E_0 + \cosh\beta\Delta_E} \\
&+\frac{1}{2}\left(1 - \frac{\sinh\beta E_0}{\cosh\beta E_0 + \cosh\beta\Delta_E}\right)\Bigg]
\end{aligned} \tag{74}$$

The matrix A is a sum of contributions proportional to the $d_a(k)$ functions. Symmetry dictates that all integrals of the form $\int d^3k d_a(k) f_c(k)$ vanish where $f_c(k)$ is any function invariant under cubic symmetry transformations. For example, $d_1(k) \sim k_y k_z$ is antisymmetric under the change of sign of either k_y or k_z. The first addend in the square bracket therefore gives no contribution to the self energy.

The second addend becomes constant for large k which leads to a divergence of the integral. However, this divergence doesn't take the form of an ϵ-peak around $d = 4$, but becomes infinite for all $d \geq 2$. This is not a problem since the correction is an irrelevant global shift of the energy levels – it can be discarded. Notably, the global shift only acquires a temperature dependence in the presence of nonzero particle-hole-asymmetry ($y \neq 0$).

The first-order terms again become zero for symmetry reasons. The antisymmetric factors in A will not be canceled by the Taylor coefficient $\propto k_i/k^4$, e. g., $d_1(k)$ will remain antisymmetric in at least one of the momentum components. The expansion of the q-dependent parts of the integral gives

$$\partial_i \partial_j \left.\frac{1}{(\vec{k}+\vec{q})^2}\right|_{q=0} = \frac{8k_i k_j}{k^6} - \frac{2\delta_{ij}}{k^4}$$
$$\frac{1}{(\vec{k}+\vec{q})^2} = (\text{lower order terms}) - \frac{q^2}{k^4} + 4\frac{(\vec{k}\cdot\vec{q})^2}{k^6} + \mathcal{O}(q^3) \qquad (75)$$

As argued for the lower-order contributions, only the specific terms "matching" the d_a will survive the integration in the addends proportional to the Γ_a. This gives the following results for the different components of the fermionic self energy defined in (71).

$$F_0^{(2)} = -2\pi e^2 \mu^\epsilon \int \frac{d^d k}{(2\pi)^d} \frac{1+4\cos^2\theta}{k^4} \frac{\sinh \beta E_0}{\cosh \beta E_0 + \cosh \beta \Delta_E} \times q^2$$
$$a = 1,2,3 : F_a^{(2)} = -4\pi e^2 \mu^\epsilon \int \frac{d^d k}{(2\pi)^d} \frac{\hat{k}_y^2 \hat{k}_z^2}{k^4 \sqrt{1+x(2+x)p_c(\hat{k})}} \frac{\sinh \beta \Delta_E}{\cosh \beta E_0 + \cosh \beta \Delta_E} d_a(q)$$
$$a = 4,5 : F_a^{(2)} = -4\pi e^2 \mu^\epsilon (1+x) \int \frac{d^d k}{(2\pi)^d} \frac{(\hat{k}_x^2 - \hat{k}_y^2)^2}{k^4 \sqrt{1+x(2+x)p_c(\hat{k})}} \frac{\sinh \beta \Delta_E}{\cosh \beta E_0 + \cosh \beta \Delta_E} d_a(q) \qquad (76)$$

The results for F_a ($a \neq 0$) are in agreement with the zero temperature case examined in section (2.3.2). For $\beta \to \infty$, the hyperbolic part becomes 1 and the anisotropy functions f_1 and f_2 remain. The momentum components inside the integral are interchangeable due to cubic symmetry which results in $F_{1/2/3}$ and $F_{4/5}$ having the same form, respectively. The F_0 component loses the temperature independent part of the residue since it has no second order contribution: The integral doesn't depend on the external momentum for the reasons outlined in section 2.3.1. It is only nonzero in the presence of particle-hole anisotropy which we won't treat in depth here. Furthermore, the temperature-dependent hyperbolic factors in the expressions for F_a with $a = 1 \ldots 5$ reduce to $\tanh(\beta\Delta_E/2)$ for $y = 0$, analogous to the bosonic self energy.

While the integration can no longer be split into a radial and an angular part, the temperature dependency can be factored out by substituting $k^2 \to \beta k^2/(2m)$

as for the bosonic self energy. This leads to a dependency proportional to $\beta^{-\epsilon/2}$ – notably, it is weak near $d = 4$. Inside the integral, the temperature results again in a regularization of the IR part while leaving the UV part responsible for the ϵ-peak untouched. Anisotropy functions $\tilde{f}_1(x)$ and $\tilde{f}_4(x)$ can be calculated with the same method as in the bosonic case – they are displayed in figure 9 and are no different from their zero temperature equivalents.

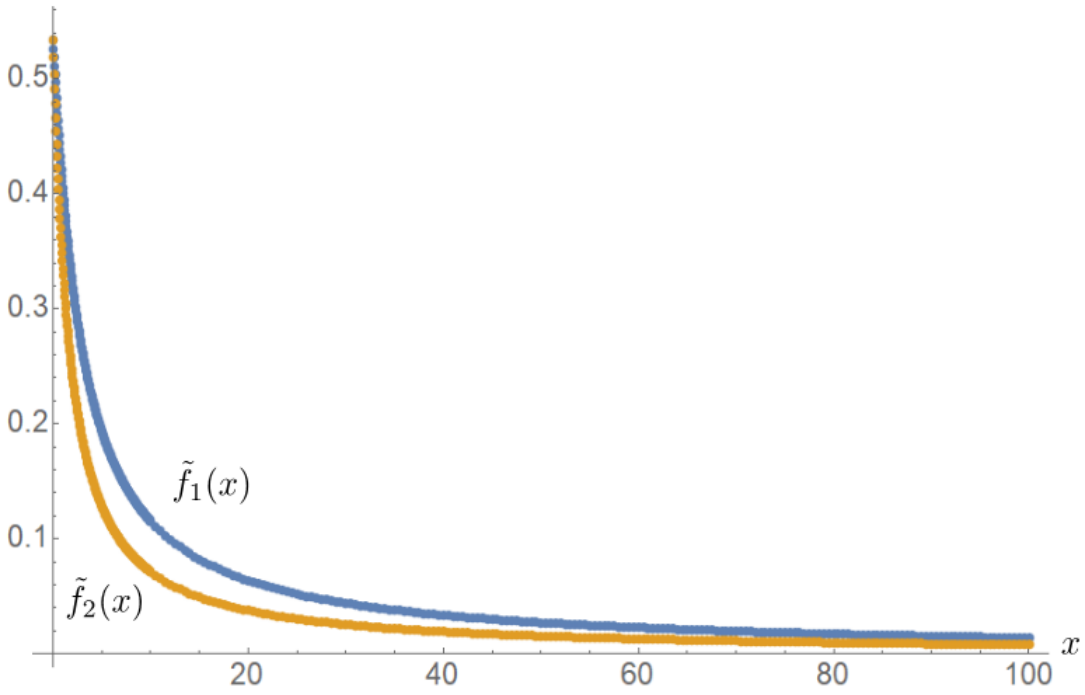

Figure 9: The anisotropy functions $\tilde{f}_1(x)$ and $\tilde{f}_4(x)$ for the bosonic self energy. They don't differ from the ones calculated for zero temperature

As in the zero temperature case, the fermionic self energy remains independent of the frequency which leads to the vertex correction vanishing.

4.2. Modified Flow Equations

The procedure goes in complete analogy to the zero temperature case in section 2.4. However, temperature acts as a new parameter in the system with canonical dimension z (the same as the frequency). The other flow equations remain unaffected up to first order in ϵ. The Z-factors need to be introduced in the same places as before and are given as follows.

$$\begin{aligned} S = \int_q \sum_\omega \Psi^\dagger(q,i\omega) \left(-i\omega + \frac{q^2}{2M_0} + Z_1 \sum_{a=1}^{3} \frac{d_a(q)\Gamma^a}{2m} + Z_4 \sum_{a=4}^{5} d_a(q)\Gamma^a \left(\frac{1}{2m} + \frac{1}{2M_c} \right) \right) \Psi(q,i\omega) \\ - ie\mu^{-\frac{\epsilon}{2}} \int_{q,k} \sum_{\omega,\Omega} \Psi^\dagger(q+k, i\omega + i\Omega)\varphi(k,i\Omega)\Psi(q,i\omega) \\ + \frac{1}{8\pi} Z_0 \int_k \sum_\Omega \varphi(-k,-i\Omega)k^2\varphi(k,i\Omega) \end{aligned} \tag{77}$$

With the results of the previous sections, they take the form

$$\tilde{Z}_0 = 1 + \frac{1}{\pi\epsilon} me^2 \tilde{f}_3(x) \tag{78}$$

$$\tilde{Z}_1 = 1 + \frac{1}{2\pi\epsilon} me^2 \tilde{f}_1(x) \tag{79}$$

$$\tilde{Z}_4 = 1 + \frac{1}{2\pi\epsilon} me^2 \tilde{f}_4(x)(1+x). \tag{80}$$

Clearly, there's no change in the rescaling when comparing to the zero temperature case since the Z factors look the same:

$$\varphi_B = \tilde{Z}_0^{\frac{1}{2}} \varphi \tag{81}$$

$$\left(\frac{1}{m}\right)_B = \tilde{Z}_1 \frac{1}{m} \tag{82}$$

$$\left(\frac{1}{m}(1+x)\right)_B = \tilde{Z}_4 \left(\frac{1}{m}(1+x)\right) \tag{83}$$

$$e_B = \mu^{-\frac{\epsilon}{2}} \tilde{Z}_3^{-\frac{1}{2}} e \tag{84}$$

All other quantities scale according to their canonical dimensions. With the

dimensionless coupling $u \coloneqq me^2/2\pi$, the β-functions ($\beta_\xi \coloneqq \mu\frac{d\xi}{d\mu}$, not to be confounded with the inverse temperature β) write the same as before. However, temperature T is now included in the parameter space.

$$\beta_{\frac{1}{m}} = (z-2)\frac{1}{m} + u\tilde{f}_1(x)\frac{1}{m} \tag{85}$$

$$\beta_y = -u\tilde{f}_1(x)y \tag{86}$$

$$\beta_x = -u(1+x)(\tilde{f}_1(x) - \tilde{f}_4(x)) \tag{87}$$

$$\beta_u = \epsilon u - (4\tilde{f}_3(x) + \tilde{f}_1(x))u^2 \tag{88}$$

$$\beta_T = zT \tag{89}$$

The known fixed point at $u_c = \epsilon/(2\tilde{f}_3(x) + \tilde{f}_1(x))$ acquires an instability in T-direction here. The formerly stable LAB fixed point is now unstable – therefore, a true zero-temperature phase cedes to exist. There may however be a region around the fixed point where LAB scaling still dominates the electronic behavior. The rest of this chapter is dedicated to identify potential regions for this to happen.

4.3. Reduced Temperature Phase Diagram

The two-dimensional parameter space is spanned by the interaction strength and temperature and exhibits an unstable fixed point at zero temperature. It is convenient to switch to canonically dimensionless quantities that isolate the anomalous flow due to the renormalization group. The natural choices are given by the dimensionless coupling u introduced earlier and a reduced temperature τ that relates the thermal energy with the characteristic energy scale of the system – since the LAB fixed point is isotropic, the only such scale is given by the band mass m.

$$u = 2\pi me^2 \tag{90}$$

$$\tau = \frac{2mT}{\mu^2} \tag{91}$$

The anomalous scaling of τ is given by

$$\beta_\tau = -\frac{8}{15} u\tau \tag{92}$$

at $x = 0$. It is displayed in figure 10(a) at $\epsilon = 1$. Figure 10(b) shows the instability of the LAB fixed point with the runaway temperature T. However, there can be low-temperature regions where the flow towards the fixed point is stronger than the runaway flow to higher effective temperature. This is the region where LAB scaling is expected to be visible in experimental data.

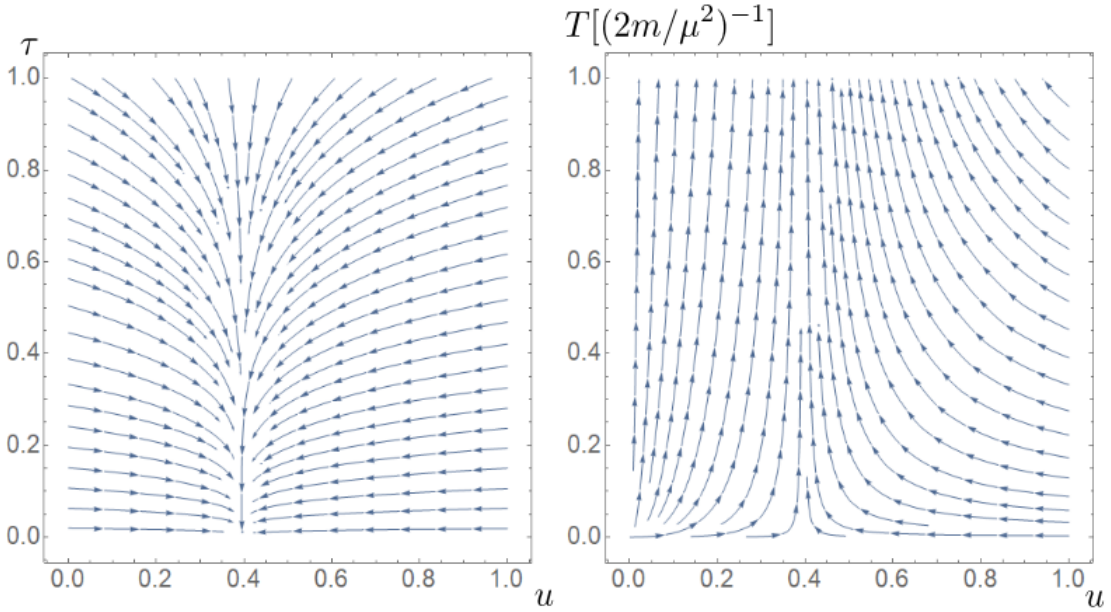

(a) Reduced temperature flow (b)Physical temperature flow

Figure 10: The RG flow in the (a) $u - \tau$ and (b) $u - T$ parameter space. Both figures are at $d = 3$, the fixed point at $u = \frac{15}{38}$ is clearly seen. The units for the physical temperature are irrelevant in principle – the ones given in the square bracket are not to be confounded with the definition of τ where those quantities counter the normal scaling.

To identify regions of different behavior in the reduced temperature flow diagram (figure 10 (a)), the characteristic temperatures estimated by Herbut et al. [9] are taken into account. To be able to generalize the flow diagrams to arbitrary

dimension, l_{LAB} from (58) needs to be generalized. As a reminder, it is the length scale emerging from comparing the free boson propagator with the q^2-part of the bosonic self energy at zero temperature:

$$1 \sim \frac{|\Sigma_\varphi(q)|}{q^2} \tag{93}$$

With the result from (26), this leads to a momentum scale μ^* and an associated length scale L^* when reinserting the physical interaction strength $\tilde{e}^2 = e^2\mu^\epsilon$:

$$\mu^* = \left(\frac{8\pi m\tilde{e}^2 f_3(x)}{\epsilon}\right)^{\frac{1}{\epsilon}} \tag{94}$$

$$L^* = \frac{1}{\mu^*} \tag{95}$$

A corresponding temperature scale T^* (and, to be precise, a reduced temperature scale τ^*) then results from comparing Coulomb energy $\tilde{e}^2/(L^*)^{d-2}$ and thermal energy T:

$$T^* = \frac{\tilde{e}^2}{(L^*)^{2-\epsilon}} \tag{96}$$

$$\tau^* = \frac{\epsilon}{4\pi}\left(\frac{4u}{\epsilon}\right)^{\frac{2}{\epsilon}} \tag{97}$$

It can be seen that in three dimensions, the reduced temperature below which Herbut et al. locate the LAB scaling goes quadratically with the interaction constant. This holds equally true for the transition temperature to a Mott ground state $T_c \approx T^*/100$ identified by them. Both temperatures are implemented in the flow diagram in figure 12.

Finally, let's determine the region affected by screening. In essence, this should confirm the estimates made in chapter 3 in the sense that screening is weak in the relevant portion of the flow diagram. To achieve this, the product $l_{scr}\mu$ is examined where μ is the momentum scale entering the reduced temperature (experimentally speaking, the momentum scale at which the effective temperature should be determined).

The region where screening is irrelevant is determined by a large screening length (compared to the characteristic length scale μ^{-1}) such that $l_{scr}\mu > 1$. After inserting all the definitions of τ and u, this estimate results in

$$\tau^{-\frac{1}{4}} u^{-\frac{1}{2}} \cdot 2.146 > 1. \tag{98}$$

This equation is valid in three dimensions. In general dimensionality, the expression for the screening length (56) is modified using the result for $\Sigma_\varphi(0)$ from (61). It reads

$$\begin{aligned} \Sigma_\varphi(0) &= C(d) m^{\frac{d}{2}} \tilde{e}^2 \beta^{1-\frac{d}{2}} \\ l_{scr} &= \frac{1}{\sqrt{C(d)}} \frac{\beta^{\frac{d}{4}-\frac{1}{2}}}{m^{\frac{d}{4}} \tilde{e}} \end{aligned} \tag{99}$$

with the dimensional factor $C(d)$ displayed in figure 11. Equation $l_{scr}\mu = 1$ then gives

$$\tau^{\frac{1}{2}-\frac{d}{4}} u^{-\frac{1}{2}} \frac{2^{\frac{d}{4}}\sqrt{\pi}}{\sqrt{C(d)}} > 1 \tag{100}$$

for the unscreened region. Qualitatively, the border of this region follows $\tau \sim u^{-2}$ in $d = 3$ and $\tau \sim u^{-1}$ in $d = 4$ with intermediate exponents in between. Quantitatively though, the whole area that is relevant for LAB scaling following the arguments of Herbut et al. lies in the unscreened region.

In conclusion, the finite temperature calculation supports the existence of a LAB scaling at one-loop level. In dimensional regularization, the temperature dependency remains largely invisible because of the UV nature of the diagram parts that diverge like $1/\epsilon$ – the Z-factors and subsequently the flow equations don't acquire temperature-dependent contributions. However, the LAB phase critical point becomes unstable in the presence of a new relevant parameter, temperature. It is probable that the nearby unstable fixed point still influences the low-temperature behavior in a certain region of the parameter plane: the zero-temperature LAB *phase* is therefore replaced by a *scaling region* gradually showing the predicted LAB properties below a crossover temperature. Screening does not seem to have a

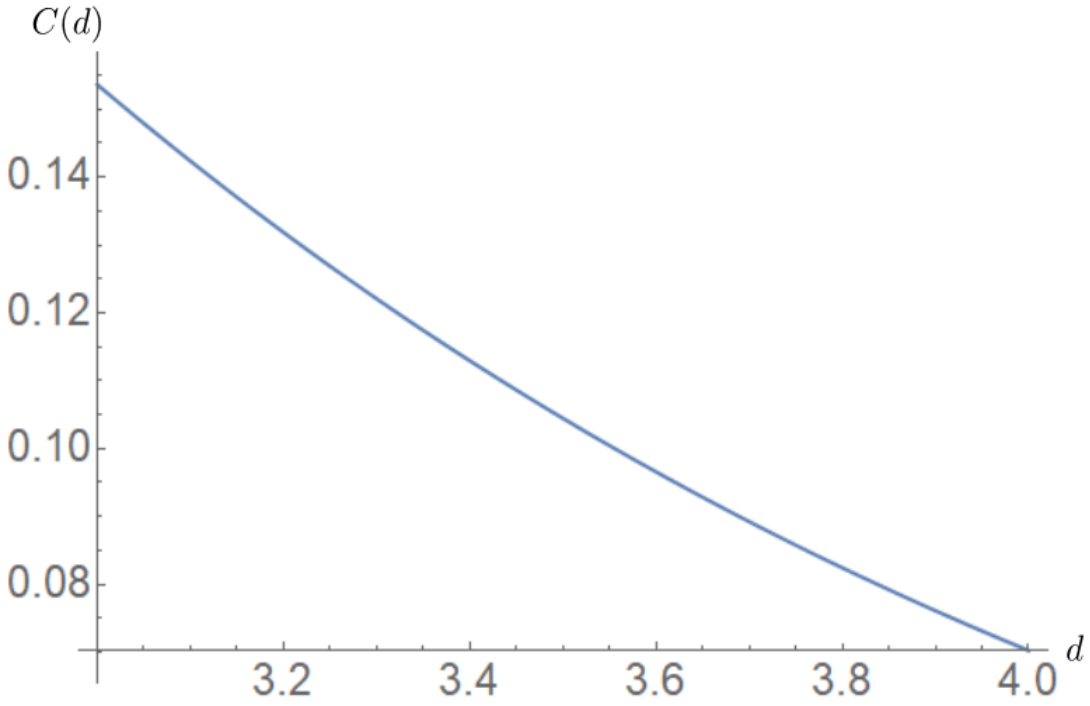

Figure 11: The dimensional factor $C(d)$ for the constant part of the bosonic self energy, entering the screening length result for a general dimension d.

significant effect in this region such that the scaling is expected to be observable.

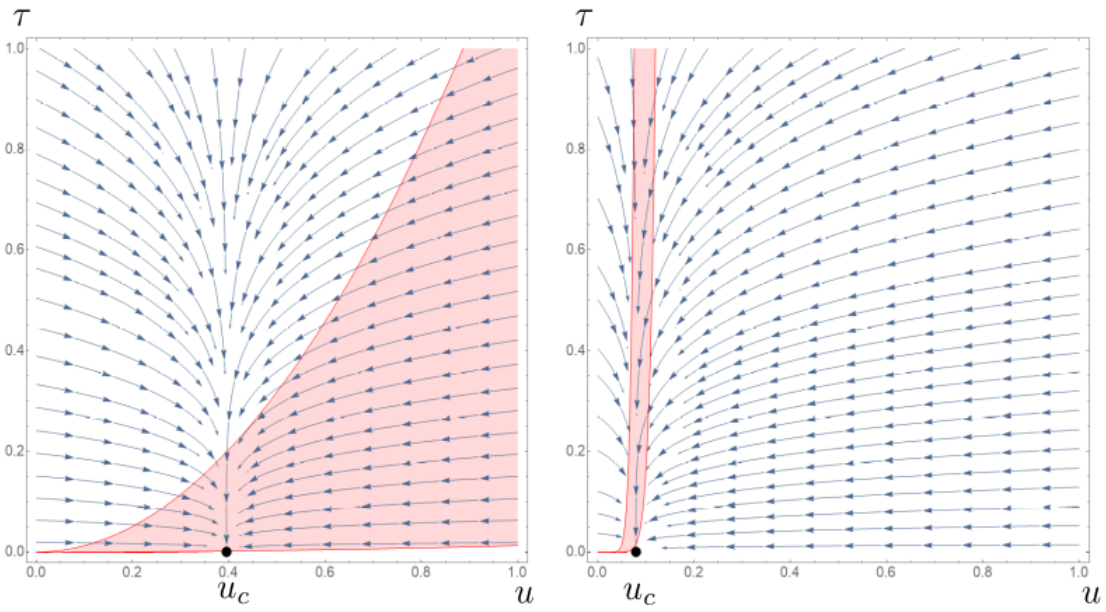

(a) d = 3 (b) d = 3.8

Figure 12: The flow diagram in the u-τ parameter plane for $d = 3$ and $d = 3.8$. The red lines represent the temperatures τ^* (upper LAB limit) and τ_c (lower LAB limit) obtained after Herbut et al. The colored region is allowed for LAB scaling. The whole plot lies within the unscreened region where $l_{scr}\mu > 1$.

5. Momentum Shell RG at Finite Temperatures

While the reasons for the invisibility of temperature in Z factors is mathematically clear, another renormalization approach can produce the dependence we're looking for. When following the original idea of passing towards larger and larger length scales by integrating out low-distance (that is to say, large momentum) degrees of freedom, temperature should eventually play a larger role once the momentum cutoff Λ and its associated energy come near the thermal energy ($E(\Lambda) \sim T$). $E(\Lambda)$ describes some energy characteristic for the system, usually given by the dispersion.

The momentum-shell renormalization program starts by imposing a general high-momentum cutoff Λ on all integrals. It proceeds by integrating out additional degrees of freedom in order to reduce the cutoff to a smaller one at Λ/b – the contribution of this momentum shell then has to be included in the effective action including valid for smaller momenta. Finally, the fields and parameters of the effective action are rescaled to restore the original form of the action. Now, both actions are built to describe the same physical system which gives rise to conditions on how the involved quantities scale with the momentum cutoff. This results in continuous flow equations when implementing the above program in infinitesimal steps $b = 1 + dl \approx e^{dl}$.

For simplicity, all calculations in this chapter will be done in the isotropic, particle-hole symmetric system. Unlike for dimensional regularization, finite contributions to the self energies (at $d = 4$) are also of interest now – this is where temperature is expected to enter the flow equations. As before, we will expand all diagrams up to second order in q. Throughout the chapter, $\Delta(\xi)$ denotes the quantity ξ with all momentum integrals only carried out over the momentum shell $[\Lambda/b, \Lambda]$.

5.1. Self Energies

The first step is the calculation of the self energies well-known by now. Most equations of the previous chapters can be recycled when properly generalized. The momentum integrals run up to a cutoff Λ and only the shell $\Lambda/b < |\vec{k}| < \Lambda$ is

needed to derive the RG flow. However, there is one complication that will alter the fermionic self energy: one needs to include a boson mass m_φ with canonical dimension 2 from the start since it will be generated by the RG flow anyway. This corresponds to replacing $q^2 \to q^2 + m_\varphi$ in the action and setting $G_\varphi = (q^2 + m_\varphi)^{-1}$ as the new bosonic Green's function.

5.1.1. Bosonic Self Energy

There are two contributions up to second order, the constant part $\Sigma_\varphi(0)$ as well as the quadratic contribution $\Sigma_\varphi^{(2)}(\vec{q})$. The former leads to a boson mass m_ϕ, effectively a screening parameter. The latter renormalizes the boson field φ.

$\Sigma_\varphi(0)$ is given by (61) evaluated at $x = y = 0$:

$$\Sigma_\varphi(0) = -\tilde{e}^2\beta \int \frac{d^dk}{(2\pi)^d} \frac{1}{1 + \cosh \frac{\beta k^2}{2m}} \delta l \tag{101}$$

The momentum shell integral then yields

$$\Delta(\Sigma_\varphi(0)) \coloneqq -\tilde{e}^2\beta \frac{S_d}{(2\pi)^d} \int_{\Lambda/b}^{\Lambda} dk k^{d-1} \frac{1}{1 + \cosh \frac{\beta k^2}{2m}} = \beta \frac{S_d}{(2\pi)^d} \Lambda^d \frac{1}{\cosh^2 \frac{\beta\Lambda^2}{4m}} \delta l \tag{102}$$

with $b = 1 + \delta l$ and $\delta l \ll 1$. The fraction $S_d/(2\pi)^d$ evaluates to $1/2\pi^2$ in three and $1/8\pi^2$ in four dimensions.

The second order contribution is given by (65). The rest terms $R(k)$ are exponentially suppressed when compared with the term proportional to $\tanh \beta k^2/4m$ and will therefore be neglected. Performing the angular integration in 3D and restoring the general dimension d afterwards following the known protocol (21) gives

$$\begin{aligned} \Delta(\Sigma_\varphi(\vec{q})) &= -8\pi m\tilde{e}^2 \frac{S_d}{(2\pi)^d S_3} \int_{\Lambda/b}^{\Lambda} dk k^{-1-\epsilon} \tanh \frac{\beta k^2}{4m} \times q^2 \\ &= -8\pi m\tilde{e}^2 \frac{S_d}{(2\pi)^d S_3} \Lambda^{-\epsilon} \tanh \frac{\beta\Lambda^2}{4m} \delta l \times q^2. \end{aligned} \tag{103}$$

5.1.2. Fermionic Self Energy

The second-order integrals for the fermionic self energy are given in (76). Its constant contributions vanish either due to antisymmetry (integrating over $d_a(k)$) or can be absorbed by a global energy shift (component $\sim \mathbb{1}$). F_0 has no second-order contribution for $y = 0$ which leaves the F_a with two independent components (e.g. F_1 and F_4). The corresponding integrals are given by

$$\begin{aligned} F_1^{(2)}(\vec{q}) &= -4\pi\tilde{e}^2 \int \frac{d^d k}{(2\pi)^d} \frac{\hat{k}_y^2 \hat{k}_z^2}{(k^2 + m_\varphi)^2} \tanh \frac{\beta k^2}{4m} d_1(q) \\ F_4^{(2)}(\vec{q}) &= -4\pi\tilde{e}^2 \int \frac{d^d k}{(2\pi)^d} \frac{(\hat{k}_x^2 - \hat{k}_y^2)^2}{(k^2 + m_\varphi)^2} \tanh \frac{\beta k^2}{4m} d_4(q). \end{aligned} \tag{104}$$

The angular integration can be resolved as usual, giving the final result

$$\begin{aligned} \Delta\left(F_1^{(2)}(\vec{q})\right) &= -\frac{16\pi}{15} \tilde{e}^2 \frac{S_d}{(2\pi)^d S_3} \frac{4\pi\Lambda^{-\epsilon}}{(1 + m_\varphi \Lambda^{-2})^2} \tanh \frac{\beta\Lambda^2}{4m} \delta l \times d_1(q) \\ \Delta\left(F_4^{(2)(\vec{q})}\right) &= -\frac{16\pi}{15} \tilde{e}^2 \frac{S_d}{(2\pi)^d S_3} \frac{4\pi\Lambda^{-\epsilon}}{(1 + m_\varphi \Lambda^{-2})^2} \tanh \frac{\beta\Lambda^2}{4m} \delta l \times d_4(q). \end{aligned} \tag{105}$$

As it should be, both contributions are equal in the $x = 0$ case.

5.2. Effective Action, Rescaling and Flow Equations

These contributions are now plugged back into (9) to get an effective action $S_<$ valid when all momentum integrations are performed with a new cutoff Λ/b:

$$\begin{aligned} S_< = \int_q \sum_\omega \Psi^\dagger(q,i\omega)\left(-i\omega + \sum_{a=1}^{5} d_a(q)\Gamma^a\left(\frac{1}{2m} + \frac{16\pi}{15}\tilde{e}^2\frac{S_d}{(2\pi)^d S_3}\frac{4\pi\Lambda^{-\epsilon}}{(1+m_\varphi\Lambda^{-2})^2}\tanh\frac{\beta\Lambda^2}{4m}\delta l\right)\right)\Psi \\ - i\tilde{e}\int_{q,k}\sum_{\omega,\Omega}\Psi^\dagger(q+k,i\omega+i\Omega)\varphi(k,i\Omega)\Psi(q,i\omega) \\ + \frac{1}{8\pi}\int_q\sum_\Omega \varphi(-q,-i\Omega)\left[q^2\left(1+8\pi m\tilde{e}^2\frac{4\pi S_d}{(2\pi)^d S_3}\Lambda^{-\epsilon}\tanh\frac{\beta\Lambda^2}{4m}\delta l\right)\right. \\ \left. + \left(m_\varphi + \beta\frac{S_d}{(2\pi)^d}\Lambda^d\frac{4\pi}{\cosh^2\frac{\beta\tilde{e}^2\Lambda^2}{4m}}\right)\right]\varphi(q,i\Omega) \end{aligned} \tag{106}$$

To restore the original cutoff Λ, fields, momenta and frequencies need to be rescaled with b according to their canonical scaling dimensions given in (12):

$$\begin{aligned} q &\to q' = bq \\ \omega &\to \omega' = b^z\omega \end{aligned} \tag{107}$$

Caution is needed when rescaling the bosonic field φ since it acquires an anomalous dimension due to the second order contribution of Σ_φ:

$$\varphi' = b^{\frac{d+z+2}{2}}\left(1 - 8\pi m\tilde{e}^2\frac{4\pi S_d}{(2\pi)^d S_3}\Lambda^{-\epsilon}\tanh\frac{\beta\Lambda^2}{4m}\delta l\right)^{\frac{1}{2}}\varphi \tag{108}$$

$$\tag{109}$$

By comparison with the original action, we find the primed equivalents of m, m_φ and $\tilde{e}$. The scaling of the interaction strength $\tilde{e}$ comes from the anomalous scaling of the boson field. When replacing $b = 1+\delta l$ again and keeping only terms up to first order in δl, they evaluate to the following set of equations where the dimensional factor $S_d/(2\pi)^d$ has been evaluated in four dimensions:

$$\begin{aligned}\frac{1}{2m'} &= (1+\delta l)^{z-2}\left(\frac{1}{2m}+\frac{2}{15\pi}\tilde{e}^2\frac{\Lambda^{-\epsilon}}{(1+m_\varphi\Lambda^{-2})^2}\tanh\frac{\beta\Lambda^2}{4m}\delta l\right)\\ &= \frac{1}{2m}+\frac{1}{2m}(z-2)\delta l+\frac{2}{15\pi}\tilde{e}^2\frac{\Lambda^{-\epsilon}}{(1+m_\varphi\Lambda^{-2})^2}\tanh\frac{\beta\Lambda^2}{4m}\delta l\end{aligned} \tag{110}$$

$$\begin{aligned}m'_\varphi &= (1+\delta l)^2\left(1+\frac{\beta\tilde{e}^2}{2\pi}\frac{\Lambda^d}{\cosh^2\frac{\beta\Lambda^2}{4m}}\delta l\right)\\ &= m_\varphi+2\delta l m_\varphi+\frac{\beta\tilde{e}^2}{2\pi}\frac{\Lambda^d}{\cosh^2\frac{\beta\Lambda^2}{4m}}\delta l\end{aligned} \tag{111}$$

$$\begin{aligned}\tilde{e}'^2 &= (1+\delta l)^{-d+z+2}\left(1+\frac{1}{\pi}m\tilde{e}^2\Lambda^{-\epsilon}\tanh\frac{\beta\Lambda^2}{4m}\delta l\right)^{-1}\tilde{e}^2\\ &= \tilde{e}^2+(\epsilon+z-2)\tilde{e}^2\delta l-\frac{1}{\pi}m\tilde{e}^4\Lambda^{-\epsilon}\tanh\frac{\beta\Lambda^2}{4m}\delta l\end{aligned} \tag{112}$$

Passing to the dimensionless interaction constant $u = m\tilde{e}^2\Lambda^{-\epsilon}/2\pi$, boson mass $\bar{m}_\varphi = m_\varphi\Lambda^{-2}$ and temperature $\bar{\beta} = \beta\Lambda^2/2m$ then results in the flow equations

$$\frac{d}{dl}\frac{1}{2m} = \left(z-2+\frac{8u}{15}\frac{1}{(1+\bar{m}_\varphi)^2}\tanh\frac{\bar{\beta}}{2}\right)\frac{1}{2m} \tag{113}$$

$$\frac{d\bar{m}_\varphi}{dl} = 2\bar{m}_\varphi+\frac{2\bar{\beta}u}{\cosh^2\frac{\bar{\beta}}{2}} \tag{114}$$

$$\frac{du}{dl} = \epsilon u-2\left(1+\frac{4}{15(1+\bar{m}_\varphi)^2}\right)\tanh\frac{\bar{\beta}}{2}u^2 \tag{115}$$

$$\frac{d\bar{T}}{dl} = \left(2-\frac{8u}{15}\frac{1}{(1+\bar{m}_\varphi)^2}\tanh\frac{\bar{\beta}}{2}\right)\bar{T}. \tag{116}$$

The three equations for the parameters in the Hamiltonian are supplemented by the flow of the reduced temperature $\bar{\beta}^{-1} = 2mT/\Lambda^2$. These equations are the central result of this thesis and completely describe the impact of finite temperature on the RG flow at one-loop level.

5.3. Discussion of the Flow

First to note, the momentum shell calculation reproduces (43) in the corresponding $\bar{T} = \bar{m}_\varphi = 0$ case.

The only fixed point of the flow equations is the well-known LAB one at $u_c = 15\epsilon/38$, $\bar{T}_c = 0$ and $m_{\varphi,c} = 0$. m defines the global energy scale which should remain fixed during the running of parameters: this results in $z = 2 - 4\epsilon/19$ at the fixed point and ensures that any observed scaling in $\bar{T}$ and u stems from T and e^2 respectively, and not from a potentially running energy scale m.

The flow in u-$\bar{T}$ parameter space (with zero boson mass) is displayed in figure 13 (a) and (b). The hyperbolic tangent doesn't introduce dramatic changes to the general structure when compared with figure 10. A shift of the "effective fixed point" of u to larger values at finite temperatures is visible, distorting the flow.

Furthermore, (c) shows the $\bar{m}_\varphi - \bar{T}$ parameter plane at $u = u_c$ and merely demonstrates the collective divergence of those parameters. In the same fashion, the $u - \bar{m}_\varphi$ flow is dominated by the runaway of $\bar{m}_\varphi$ as displayed in (d).

The coupled differential equations cannot be solved analytically, but we can compute numerically how the bosonic mass $\bar{m}_\varphi(l = \infty)$ at the end of the flow depends on the initial temperature $\bar{T}(l = 0)$. This allows us to compare the result with the screening length approach made in chapter 3 which resulted in $m_\varphi \sim 1/l_{scr}^2 \sim \sqrt{T}$.

We proceed as follows: We find numerical solutions for the flow equations starting at initial values $\bar{m}_\varphi(0) = 0$, $u(0) = u_0$ and $\bar{T}(0) = t_0$. Varying t_0 when keeping u_0 fixed, we then plot $\bar{m}_\varphi(l \gg 1)$ against t_0 and fit a function at_0^b to the data to find the exponent B. To check whether there is any u_0 dependence in the exponent, we repeat this procedure for multiple starting values u_0. It turns out that B is independent of u_0.

As a check, the RPA result from chapter 3 can be reproduced by neglecting all anomalous flow terms in $\bar{T}$ and u. Figure 14 shows the fits using (a) the simplified flow equations and (b) the full ones. The exponent evaluates to $b \approx 1.1$ for small initial values t_0. Thus, the anomalous temperature and interaction flow increases the screening strength when compared with the RPA approach.

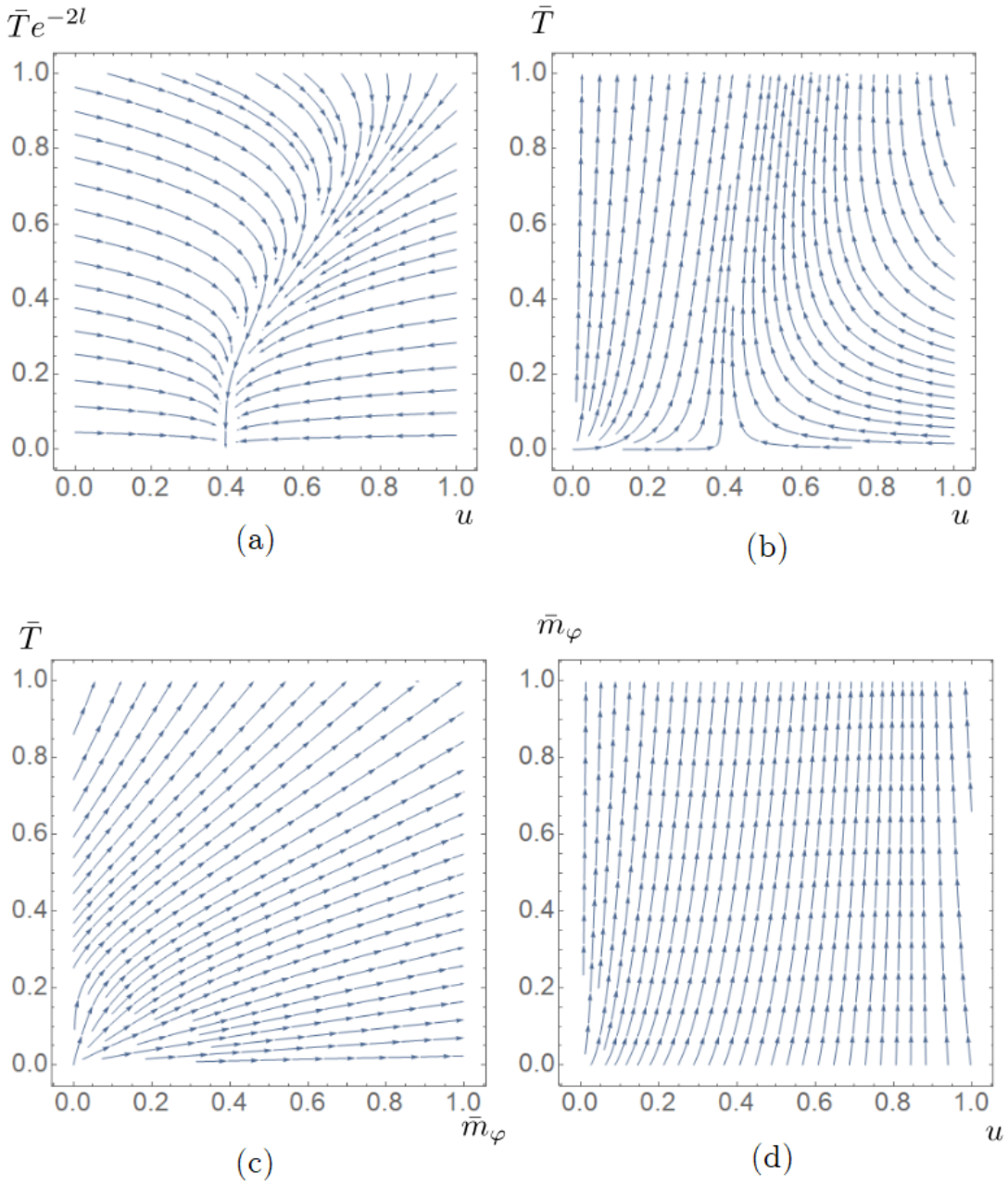

Figure 13: The flow diagrams originating in the momentum shell approach. (a) and (b) show the $u - \bar{T}$ plane where the normal scaling of the temperature has been factored out in (a) while (b) includes it. (c) shows the $\bar{m}_\varphi - \bar{T}$ and (d) the $u - \bar{m}_\varphi$ plane. Both diagrams are dominated by the divergence of $\bar{m}_\varphi$ and $\bar{T}$.

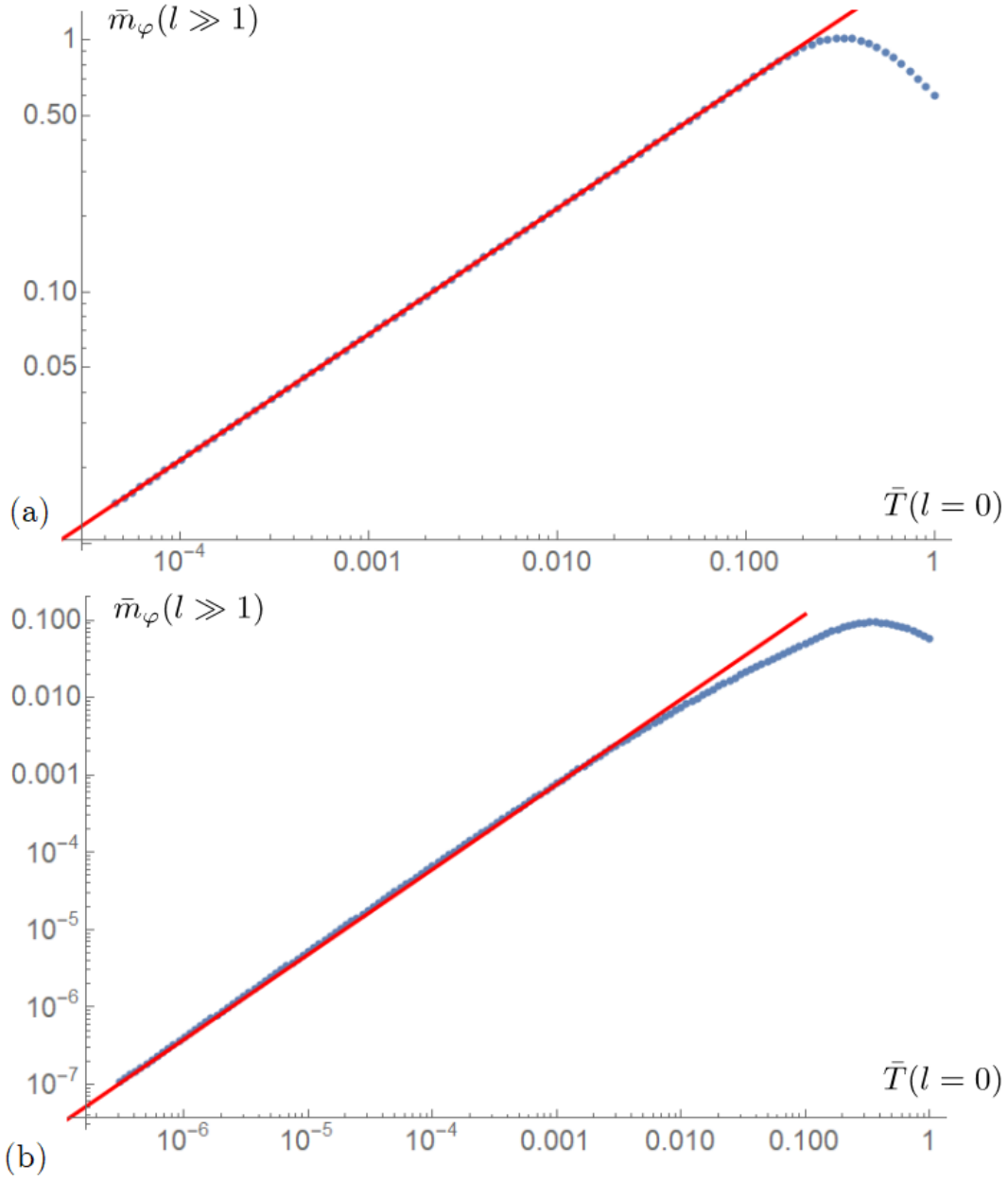

Figure 14: $\bar{m}_\varphi(l \gg 1)$ over $\bar{T}(l=0)$ together with a fit of the form $a(\bar{T}(0))^b$ (red line). (a) is obtained using the simplified flow equations neglecting the anomalous flow of the temperature and the interaction constant and has $b = 1/2$. (b) shows the results for the full flow equations (114) through (116) with $b \approx 1.1$. The exponent b is independent of $u(l=0)$ in both cases.

6. Discussion

Finally, let's recapitulate the calculations and discuss the results while linking the different chapters. We started with the calculation leading to the LAB fixed point made by Moon et al. [2] with the goal of extending its results to finite temperature and examining the fate of the LAB fixed point. The problem was tackled from three angles: First, a random phase approximation has been used to calculate the screening length confining the Coulomb interaction at finite temperature and to compare it with the characteristic LAB length scale identified by Herbut and Janssen [9]. We found their ratio to indicate the screening to be irrelevant since $l_{scr} \gg l_{LAB}$ by a factor of around 10^2 for reasonable choices of the interaction strength and band mass. Due to the relatively weak $T^{-1/4}$ scaling of l_{scr}, this hierarchy holds over the entire temperature window for the observation of LAB scaling obtained in [9] and beyond.

Second, the natural extension of the calculation in [2] has been made in chapter 4. Within the dimensional regularization approach, the temperature doesn't alter the RG flow of the existing parameters when correctly absorbing the IR divergence – only the small momentum (large distance) modes are affected by temperature and the UV divergence is left untouched. The RG flow does include temperature as an additional parameter however, with a scaling dimension $z = 2 - 4\epsilon/19 > 0$ at the critical point. The LAB fixed point therefore becomes unstable and one is left with a runaway flow towards the high-temperature Fermi liquid phase. The existence of a crossover region where the LAB scaling (that is to say, the scaling of physical quantities with the critical exponents at the LAB fixed point) is possible and not suppressed by finite temperature effects.

Third, the momentum shell approach led to flow equations including both a finite boson mass m_φ generated during the procedure and incorporated temperature-dependent factors such as $\tanh \beta\Lambda^2/(2m)$ in the RG flow. The results were in agreement with the dimensional regularization approach when setting the temperature and boson mass to zero. Their fixed point structure is unaltered. The boson mass m_φ was shown to scale approximately as $T(0)^{1.1}$ in contrast with $T^{1/2}$ from chapter 3. Screening is therefore reinforced in the LAB model and the RPA doesn't produce correct results at one-loop level when it comes to the renormalization of

the Luttinger Hamiltonian.

All calculations hint towards the fixed point scaling being visible in the temperature window derived by Herbut and Janssen [9] considering the borders to other phases generated by additional interactions. Finite temperature does indeed destroy the stability of the fixed point though: both the temperature and the boson mass generated in the momentum shell approach ultimately diverge.

The dimensional regularization scheme showed no temperature dependence in the flow equations where the momentum shell procedure did. There are two reasons for this. First, the diverging parts of the integrals treated in dimensional regularization acquired temperature-dependent factors such as $\tanh \beta k^2/4m$. For large k, they converge to 1 and are therefore irrelevant for the UV part of the integral which is responsible for the ϵ-peak. Including finite counterterms would indeed have introduced a temperature dependence. The momentum shell approach is fundamentally different because it starts with a cutoff Λ on all momentum integrals. Thus, the temperature factor always plays a role determined by the ratio of thermal energy to the cutoff energy $\Lambda^2/2m$. Second, the momentum shell integrals did not drop finite terms such as the constant part of the bosonic self energy. This results in a finite boson mass being generated even if zero in the original action. As it should be, this boson mass turns out to be closely related to temperature: it will only be newly generated at finite T, and both quantities diverge simultaneously during the RG flow. Of course, both renormalization schemes are still compatible in the sense that they generate the same fixed points and the same relevant and irrelevant parameters.

The anisotropy x has only been included in the dimensional regularization approach, however, the momentum shell integrals will contain similar anisotropy functions $f_i(x)$. A finite value $x \neq 0$ seems to assist the LAB scaling as argued in the length scale hierarchy in section 3. However, it shouldn't be forgotten that it remains an irrelevant RG parameter that will flow to zero at the LAB fixed point. This justifies the focus on the isotropic system in the momentum shell calculation.

When seeking to expand the results of this thesis, it could be valuable to include the additional contact interactions $g_1(\Psi^\dagger\Psi)^2$ and $g_2(\Psi^\dagger\Gamma_a\Psi)^2$ by Herbut and Janssen [9] in a similar finite temperature calculation. Higher-order terms are unlikely to change the picture drastically, but could be explored for example to

check how the vertex correction (vanishing at first order) influences the flow in the interaction strength.

Appendices

A. Matsubara Sum Evaluation

This section will give a brief explanation of how sums over Matsubara frequencies are resolved in this thesis. The main principle is described in [12, p.170-171]. The goal is to calculate sums like

$$S = \sum_{\omega_n} f(i\omega_n) \tag{117}$$

with the ω_n being either fermionic or bosonic Matsubara frequencies ($n \in \mathbb{Z}$):

$$\omega_n = \begin{cases} \frac{(2n+1)\pi}{\beta} & \text{if fermionic} \\ \frac{2n\pi}{\beta} & \text{if bosonic} \end{cases} \tag{118}$$

The sum can then be transformed into an integral using that these frequencies are where the poles of $n_F(i\omega)$ and $n_B(i\omega)$ are located. These poles have the residue $\zeta\frac{1}{\beta}$ with $\zeta = 1$ for bosonic frequencies and $\zeta = -1$ for fermionic ones.

$$n_{F/B}(z) = \frac{1}{e^{\beta z} \pm 1} \tag{119}$$

Therefore, S can be expressed as contour integral over the $\mathcal{C}_1$ in figure 15, using the residue theorem in reverse. Conversely, the "infinite circle" path $\mathcal{C}_2$ contains all poles of both $n_{F/B}(z)$ and $f(z)$. Because the integrand is exponentially suppressed for large z, the sum of the residues at all these poles is zero: it follows that S can be written as sum over the residues at the poles of $f(z)$ alone, or equivalently as contour integral over $\mathcal{C}_3$:

$$S = \zeta\beta \oint_{\mathcal{C}_1} \frac{dz}{2\pi i} f(z) n_{F/B}(z) \tag{120}$$

$$= \zeta\beta \oint_{\mathcal{C}_2} \frac{dz}{2\pi i} f(z) n_{F/B}(z) - \beta \oint_{\mathcal{C}_3} \frac{dz}{2\pi i} f(z) n_{F/B}(z) \tag{121}$$

$$= -\zeta\beta \oint_{\mathcal{C}_3} \frac{dz}{2\pi i} f(z) n_{F/B}(z) \tag{122}$$

$$= -\zeta\beta \sum_{\text{poles of f}} \text{Res}(f(z) n_{F/B}(z)) \tag{123}$$

When used in the thesis, it will be understood that the intermediate steps involving $\mathcal{C}_1$ and $\mathcal{C}_2$ will be skipped and all complex contour integrals involving fermionic or bosonic occupation functions $n_{F/B}(z)$ are to be understood with contour $\mathcal{C}_3$ unless otherwise specified.

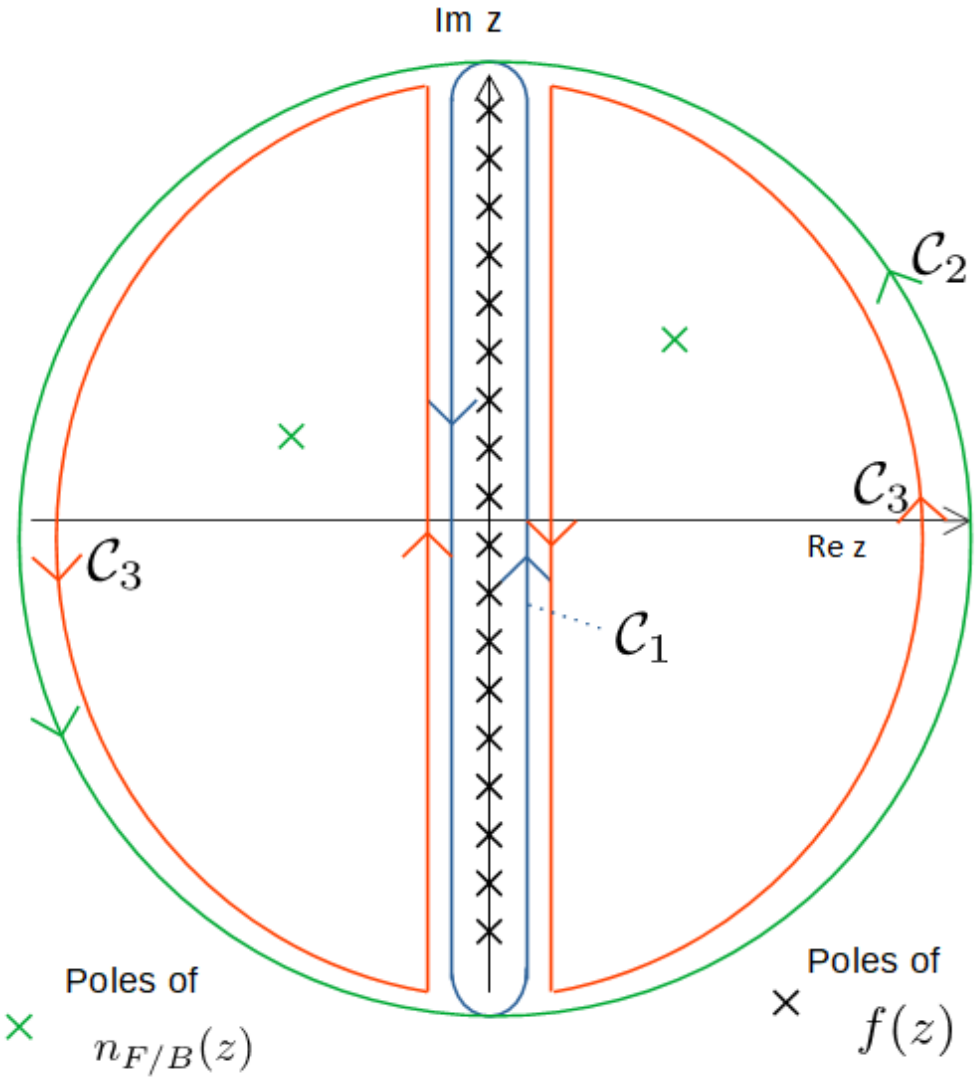

Figure 15: Overview over the relevant contours for Matsubara summation. $\mathcal{C}_1$ includes the poles at Matsubara frequencies, $\mathcal{C}_2$ both those and the poles of $f(z)$ and $\mathcal{C}_3$ only the poles of $f(z)$.

B. Fermionic Self Energy and Vertex Correction - A Ward Identity

To avoid the explicit calculation of the vertex correction $\gamma(\vec{k}, \vec{k'}, \omega, \omega')$ in the main text, it was mentioned that frequency independence of the fermionic self energy causes it to become zero. This section will give a brief explanation of the Ward identity leading to this result. For briefness and because no other case is needed, all work is done at one loop level.

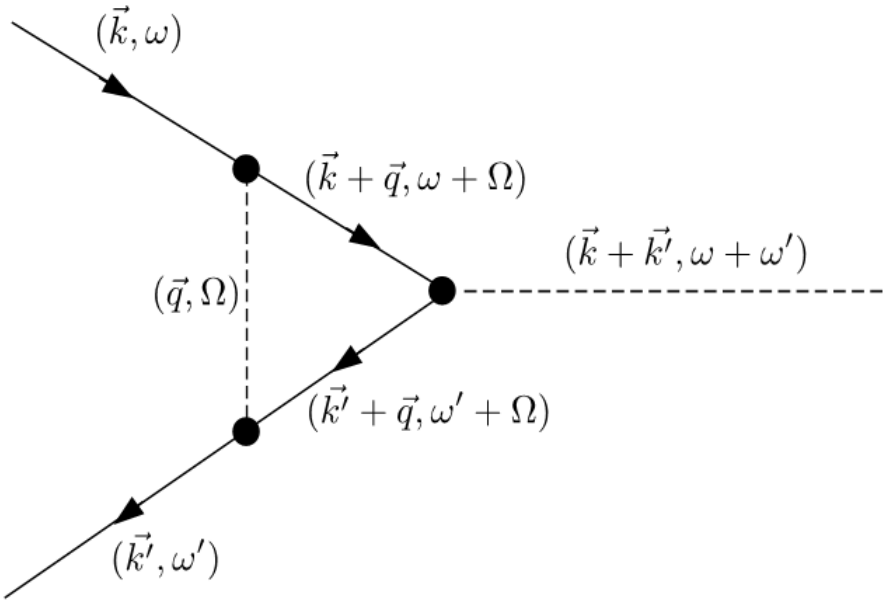

Figure 16: The vertex correction. Dashed lines represent bosonic Green's functions, unbroken ones are fermionic. The bosonic Green's function is independent of frequency, the designations on the dashed lines are given only for completeness.

It will be shown that the diagonal part of the vertex correction $\gamma(\vec{k}, \vec{k}, \omega, \omega)$ is proportional to the partial derivative of the self energy with respect to frequency. The starting point is the same derivative of the fermionic Green's function:

$$\frac{\partial}{\partial\omega}G_f(\vec{k},\omega) = \frac{\partial}{\partial\omega}(i\omega - H(\vec{k}))^{-1} = -i(i\omega - H(\vec{k}))^{-2} = -i(G_f(\vec{k},\omega))^2 \tag{124}$$

Given that the bosonic Green's function doesn't depend on frequency, it follows

$$\begin{aligned}\frac{\partial}{\partial\omega}\Sigma_f(\vec{k},\omega) &= e^2\mu^{-\epsilon}\int_{q,\Omega}\frac{\partial}{\partial\omega}G_f(\vec{k}+\vec{q},\omega+\Omega)G_\varphi(\vec{q}) &(125)\\ &= -ie^2\mu^{-\epsilon}\int_{q,\Omega}(G_f(\vec{k}+\vec{q},\omega+\Omega))^2G_\varphi(\vec{q}) &(126)\\ &= -i\gamma(\vec{k},\vec{k},\omega,\omega). &(127)\end{aligned}$$

Therefore, if the fermionic self energy is independent of the external frequency, $\gamma(\vec{k},\vec{k},\omega,\omega)$ vanishes.

C. Complete Form of the Bosonic Anisotropy Function

The bosonic anisotropy function $f_3(x)$ encapsulates the dependency of the bosonic self energy on the anisotropy parameter x in the zero temperature case (section 2.3.1) and is assumed to extend in a similar form to finite temperature (section 4.1.1):

$$\begin{aligned}f_3(x) = \frac{3}{8\pi}\int_{-1}^{1}dc\int_0^{2\pi}d\phi\frac{6\sqrt{2}s^2}{\left(\sqrt{1+x(2+x)p_c(\hat{k})}\right)^5}\times\\ \Big[8-2x(7c^4-10c^2-5)-x^2(23c^4-26c^2-5)\\ +16c^2s^2(c^3-4c^2s^2x^4-s^2x(2+x))(3+x^2(1+4x(2+x)\cos 4\varphi))\Big] \qquad (128)\end{aligned}$$

Here, the abbreviations $c = \cos\theta$ and $s = \sin\theta$ have been used in addition to the ones in the main text. To find the asymptotic form given there, only terms of order x^4 are kept in the numerator – all others will vanish in the limit of large x.

References

[1] J. M. Luttinger, "Quantum theory of cyclotron resonance in semiconductors: general theory", Phys. Rev. **102**, 1030–1041 (1956).

[2] E.-G. Moon, C. Xu, Y. B. Kim, and L. Balents, "Non-fermi-liquid and topological states with strong spin-orbit coupling", Phys. Rev. Lett. **111**, 206401 (2013).

[3] A. A. Abrikosov and Beneslavsky, "Possible existence of substances intermediate between metals and dielectrics", Soviet Physics JETP **32**, 699–708 (1971).

[4] A. A. Abrikosov, "Calculation of critical indices for zero-gap semiconductors", Soviet Physics JETP **39**, 709–716 (1974).

[5] K. G. Wilson and M. E. Fisher, "Critical exponents in 3.99 dimensions", Phys. Rev. Lett. **28**, 240–243 (1972).

[6] G. 't Hooft, "Dimensional regularization and the renormalization group", Nuclear Physics B **61**, 455–468 (1973).

[7] S. Weinberg, "New approach to the renormalization group", Phys. Rev. D **8**, 3497–3509 (1973).

[8] S. Murakami, N. Nagosa, and S.-C. Zhang, "SU(2) Non-abelian holonomy and dissipationless spin current in semiconductors", Phys. Rev. B **69**, 235206 (2004).

[9] I. F. Herbut and L. Janssen, "Topological mott insulator in three-dimensional systems with quadratic band touching", Phys. Rev. Lett. **113**, 106401 (2014).

[10] L. Janssen and I. F. Herbut, "Nematic quantum criticality in three-dimensional fermi system with quadratic band touching", Phys. Rev. B **92**, 045117 (2015).

[11] I. Boettcher and I. F. Herbut, "Anisotropy induces non-fermi-liquid behavior and nematic magnetic order in three-dimensional luttinger semimetals", Phys. Rev. B **95**, 075149 (2017).

[12] A. Altland and B. D. Simons, *Condensed matter field theory*, 2nd ed. (Cambridge University Press, 2010).

[13] I. Mandal, “Search for plasmons in isotropic luttinger semimetals”, Annals of Physics **406**, 173–185 (2019).

Declaration

I hereby declare that this thesis is my own work, and that I have not used any sources and aids other than those stated in the thesis.

Munich, 3rd February 2021

Benedikt Poggel